Paleomagnetic directions and $^{40}Ar/^{39}Ar$ ages from the Tatara-San Pedro volcanic complex, Chilean Andes: Lava record of a Matuyama-Brunhes precursor?

Laurie L. Brown,[1] Brad S. Singer,[2] James C. Pickens,[1,3] and Brian R. Jicha[2]

Received 4 February 2004; revised 6 July 2004; accepted 30 August 2004; published 3 December 2004.

[1] Lava flows within Quebrada Turbia valley of the Tatara San Pedro volcanic complex, in central Chile (36°S, 289°E), preserve a detailed record of what was presumed to be the Matuyama-Brunhes geomagnetic reversal. A sampling traverse in the central west wall of the valley yields reverse and transitional polarity flows of the Quebrada Turbia sequence. Two kilometers to the north, another section yields 17 transitional flows from the same volcanic sequence overlain by flows with normal polarity. The $^{40}Ar/^{39}Ar$ incremental heating experiments on lavas within the two sections provide nine independent age determinations and yield a weighted mean of 791.7 ± 3.0 ka (±2σ) for the paleomagnetic transition. The sections are linked by geological mapping, the precise radioisotopic dating, and geochemical correlations. Alternating field and thermal demagnetization studies, rock magnetic analyses, and petrographic observations indicate that the magnetization is primary and carried by titanomagnetite. The polarity change is characterized by a jump from reverse poles to a quasi-stationary cluster of virtual geomagnetic poles over Australia, followed by a jump to normal polarity latitudes. Magnetization of these lavas is thus consistent with either a brief period when the field was dominated by a subequatorial dipole, or a more complex nondipolar field that may reflect the influence of a long-lived regional lower mantle control over a weakened dynamo. The Quebrada Turbia lavas are circa 16 kyr older than those, dated by exactly the same methods, which record a later more complex portion of the reversal at Haleakala volcano, Maui. Moreover, the 792 ka radioisotopic age of these Chilean lavas is older than most astronomical estimates for the Matuyama-Brunhes reversal suggesting that this section may, in fact, record a precursor to the actual field reversal, that is expressed by low paleointensities in more than a dozen well-studied marine sediment cores. *INDEX TERMS:* 1535 Geomagnetism and Paleomagnetism: Reversals (process, timescale, magnetostratigraphy); 1030 Geochemistry: Geochemical cycles (0330); 9360 Information Related to Geographic Region: South America; 9604 Information Related to Geologic Time: Cenozoic; *KEYWORDS:* paleomagnetism, reversal, geochronology, Andes, lavas, $^{40}Ar/^{39}Ar$ dating

Citation: Brown, L. L., B. S. Singer, J. C. Pickens, and B. R. Jicha (2004), Paleomagnetic directions and $^{40}Ar/^{39}Ar$ ages from the Tatara-San Pedro volcanic complex, Chilean Andes: Lava record of a Matuyama-Brunhes precursor?, *J. Geophys. Res.*, *109*, B12101, doi:10.1029/2004JB003007.

1. Introduction

[2] Debate in the paleomagnetic community has recently focused on the nature of magnetic polarity reversals and what implications these field changes have with respect to deep earth processes [*Merrill and McFadden*, 1999]. Unfortunately, realistic modeling of the Earth's magnetic field in its transitional state remains elusive. This is not only a testament to the difficulties in modeling such a complex system, but it is also a function of the conflicting and incomplete nature of data sets that provide constraints for such models [*Coe and Glen*, 2004]. In particular, virtual geomagnetic pole (VGP) paths, which are traditionally used to map transitional field geometries, are commonly incomplete, not well constrained geochronologically, and typically offer contradictory data for individual reversals. In some analyses of the global reversal database, VGP patterns are interpreted to be unequivocal and to demonstrate definitive paths that have repeated during numerous reversal transitions for the past 10 million years [*Clement*, 1991; *Laj et al.*, 1991; *Tric et al.*, 1991, *Love and Mazaud*, 1997] or that transitional data has clustered at specific spots on the Earth's surface [*Hoffman*, 1992, 1996]. In other analyses, treatments of similar but older (<12 Ma) data [*Valet et al.*, 1992],

[1]Department of Geosciences, University of Massachusetts, Amherst, Massachusetts, USA.
[2]Department of Geology and Geophysics, University of Wisconsin, Madison, Wisconsin, USA.
[3]Now at ExxonMobile Exploration Company, Houston, Texas, USA.

0148-0227/04/2004JB003007$09.00

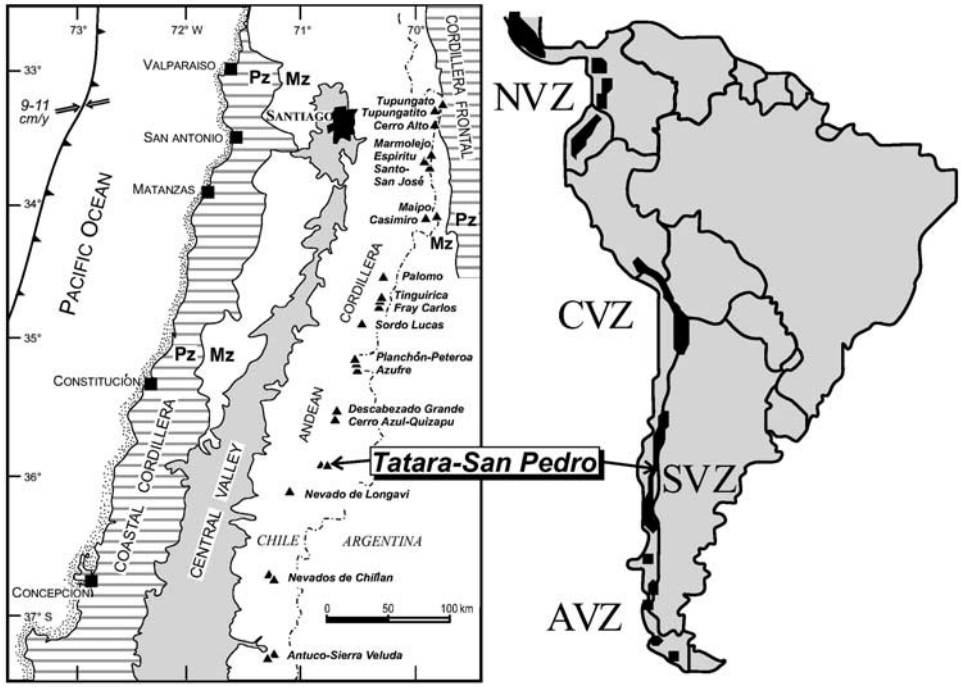

Figure 1. Site location (36°S, 71°W) of the Tatara-San Pedro volcanic complex, Chile. Locations of other arc volcanoes of the Southern Volcanic Zone (SVZ) are also shown. Abbreviations are as follows: NVZ, Northern Volcanic Zone; CVZ, Central Volcanic Zone; AVZ, Austral Volcanic Zone.

or subsets of these data [*Prevot and Camps*, 1993], discern no patterns at all, suggesting random field behavior for successive polarity changes. Furthermore, even if the two antipodal VGP paths are real, it is not clear from these data as to whether the geomagnetic field remains dipolar during reversals or reduces in some manner to a nondipolar field.

[3] Considerable progress on three-dimensional dynamo simulations [*Glatzmaier and Roberts*, 1995; *Kuang and Bloxham*, 1997] notably includes models comprising spontaneous reversals [*Glatzmaier et al.*, 1999; *Coe et al.*, 2000]. If coupling between the outer core and lower mantle has affected the geodynamo as these authors suggest, paleomagnetic data provide an independent and long-term record of this interaction. It is therefore imperative that reversal geometries are more clearly defined. In this regard, it would seem prudent that the nature of individual reversals be understood first, before trends for multiple transitions can be compared and rigorously evaluated. The most recent reversal, the Matuyama-Brunhes, may provide the best opportunity to eventually gain a spherical harmonic expression of a transitional field. It is the most documented reversal and at the present time the best defined [*Clement*, 1991; *Love and Mazaud*, 1997; *Hoffman*, 2000].

[4] Here we report on detailed paleomagnetism and geochronology of what was previously assumed to be the Matuyama-Brunhes transition recorded in an arc volcano of the Chilean Andes [*Brown et al.*, 1994; *Singer and Pringle*, 1996; *Singer et al.*, 1997]. Thirty basaltic andesite flows, from two correlative sections located within a canyon cutting the Tatara-San Pedro volcanic complex (TSPVC) of central Chile [*Singer et al.*, 1997], carry a record that is exceptionally well constrained temporally and geochemically as well as paleomagnetically. These flows record an abrupt change from reversed polarity to a period of transitional stability, with virtual geomagnetic poles clustered geographically over Australia, followed by another abrupt swing to normal polarity, and appear to represent a precursor to the actual reversal.

2. Geologic Setting

2.1. Tatara-San Pedro Volcanic Complex

[5] The Tatara-San Pedro volcanic complex is a Quaternary frontal arc volcano located within the central section of the Southern Volcanic Zone of the Chilean Andes at 36°S (Figure 1). Nearly one million years of geologic activity is represented in the edifice, which is characterized by geochemically related batches of lavas separated in space by paleotopography and in time by erosional and magmatic hiatuses [*Ferguson et al.*, 1992; *Dungan et al.*, 1992; *Singer et al.*, 1997; *Dungan et al.*, 2001]. Magmatic compositions include basalts, rhyolites, and dacites, but approximately two thirds of the erupted volume consists of mafic andesite [*Singer et al.*, 1997]. Rapid regional uplift combined with glacial scouring and fluvial erosion has produced deeply incised canyons radial to and across the complex, providing up to 1 km deep cross-sectional exposure of the local geology (Figures 2 and 3). These canyons provide access to vertical sections throughout the edifice, offering continuous sampling from the cap of Holocene flows through to Miocene basement rocks. Field relations, paleomagnetic studies, and radioisotopic dating have led to the subdivision of the volcanic complex into 17 distinct chronostratigraphic units, described by *Singer et al.* [1997]. These units have been further refined using extensive geochemical data by *Dungan et al.* [2001]. A simplified geologic map is presented in Figure 2 in which units younger than 600 ka have been lumped into two categories, deposits from Volcan San

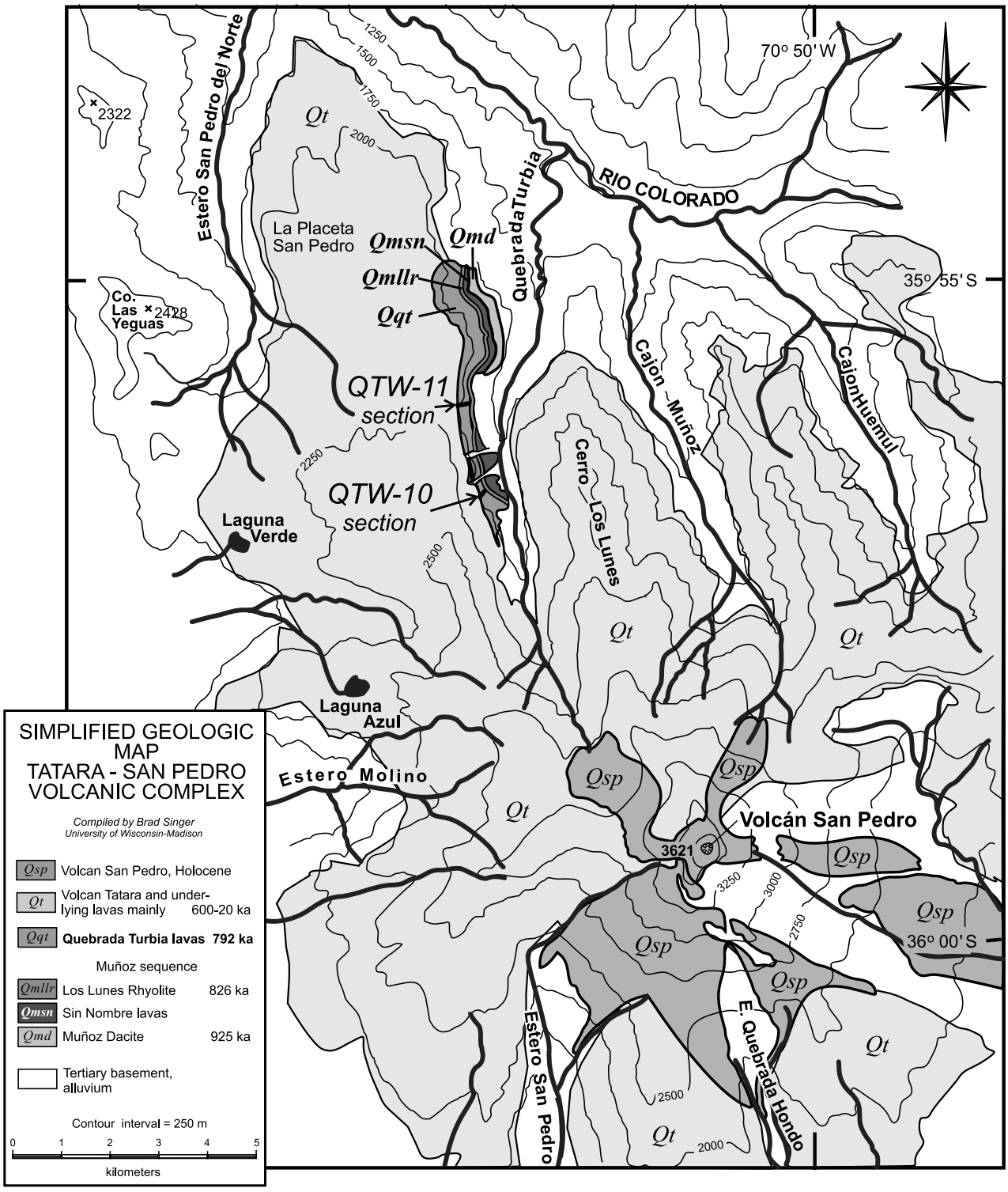

Figure 2. Simplified geologic map of the Tatara-San Pedro volcanic complex, Chile. Locations of sections QTW-10 and QTW-11, discussed in the text, are indicated by arrows. Map is modified from *Singer et al.* [1997]. See color version of this figure at back of this issue.

Pedro (Qsp), Holocene in age, and deposits from Volcan Tatara (Qt) and the underlying flows. Below the Volcan Tatara flows lie the Quebrada Turbia lavas (Qqt), the subject of this paper. These lavas are found above the Munoz sequence, comprising the Los Lunes Rhyolite (Qmllr) with an age of 826 ka, [*Singer and Pringle*, 1996; *Singer et al.*, 1997], the Sin Nombre lavas (Qmsn) and the Munoz Dacite (Qmd), 925 ka [*Singer et al.*, 1997].

2.2. Quebrada Turbia

[6] Samples for this study were collected from flows exposed within Quebrada Turbia, a deeply incised canyon

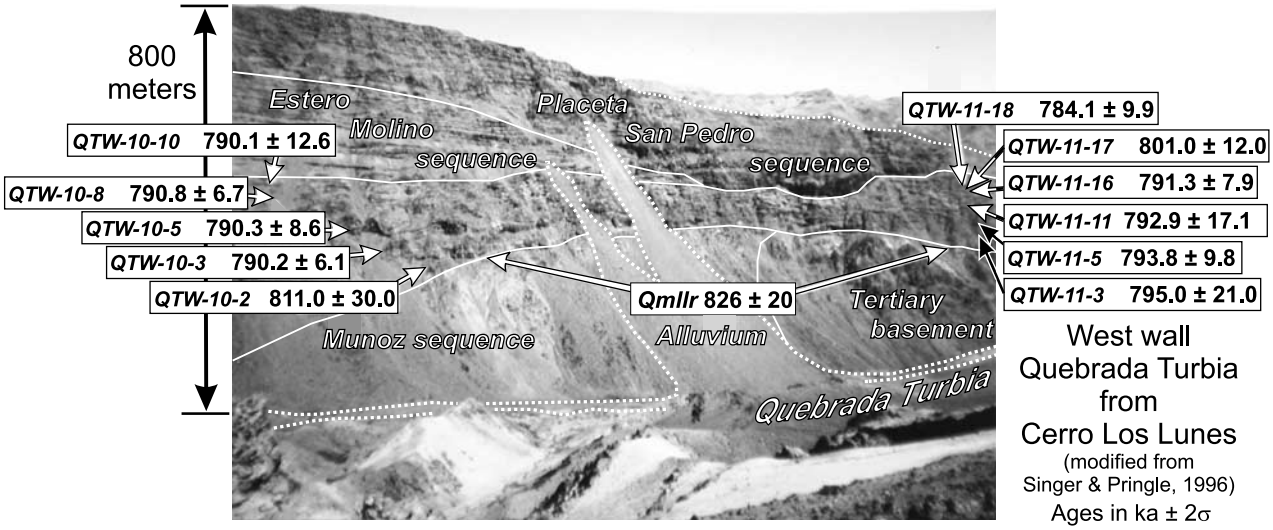

Figure 3. Photograph of the west wall of Quebrada Turbia. Vertical relief from the valley floor to ridge is ~800 m. Sequences above and below the Quebrada Turbia sequence are labeled. Location of 12 radioisotopic age determinations and associated paleomagnetic sites are indicated. Paleomagnetic sites are numbered from the bottom up; section QTW-10, sites 10-1 to 10-11 are on the left, and section QTW-11, sites 11-1 to 11-20 are on the right and were collected in traverses joining and coincident with the radioisotopic locations. See Table 2 for additional information on the age determinations. See color version of this figure at back of this issue.

on the north side of the Volcan San Pedro edifice (Figure 2). Geological exposure is essentially uninterrupted in the ravine, with only minor vegetation and occasional scree cover. The west wall of the canyon provides an 800 m vertical cross section through west-northwest gently dipping lava flows that sit unconformably on metamorphosed beds of Miocene age (Figure 3).

[7] The volcanic stack is cut by three angular unconformities, separating the west wall into four distinct temporal packages ranging in age from 975 to 250 ka [*Singer et al.*, 1997]. The oldest lavas exposed, represented by one basaltic-andesite flow and an overlying clastic unit, belong to the Sin Nombre lavas of the Munoz sequence (925 – 820 ka). Lavas of Quebrada Turbia sequence (~793 ka), which are the focus of this study, sit unconformably on the clastic unit and are truncated above, along major unconformities. This unconformity separates the Quebrada Turbia units from the overlying Estero Molino sequence, which ranges in age from 605 to 330 ka. Higher in the section, another major unconformity separates Estero Molino lavas from overlying basalts of the Placeta San Pedro sequence (circa 230 ka), the youngest lavas exposed in the canyon.

[8] Two sampling traverses, QTW-10 (medial section) and QTW-11 (distal section), were conducted on the west wall of Quebrada Turbia [*Singer and Pringle*, 1996] (Figure 3). All four volcanic sequences were sampled in section QTW-10 in a continuous traverse from the base of the canyon to its rim. A single Sin Nombre lava (QTW-10-1), of the Munoz sequence, lies at the bottom of this section and is separated from overlying Quebrada Turbia flows by a clastic unit containing blocks of Los Lunas Rhyolite (826 ka) [*Singer et al.*, 1997]. Ten Quebrada Turbia lavas crop out before the next unconformity in the section. Above this unconformity, representing a ~450 kyr break in the stratigraphy, lie 18 flows of the Estero Molino group followed by the next unconformity, and then 20 Placeta San Pedro sequence flows. Section QTW-10 as reported here contains one lava of the Sin Nombre sequence at the base, ten lavas of the Quebrada Turbia sequence, and then only the first lava (QT-10-12) of the younger Estero Molino sequence.

[9] Section QTW-11 contains an expanded package of Quebrada Turbia lavas, but without Estero Molino flows present (Figure 3). At the base of QTW-11 the same Munoz clastic unit observed in QTW-10 rests on metamorphosed Miocene basement rocks and is overlain by Quebrada Turbia lavas, with no Sin Nombre lavas present. The unconformity separating Quebrada Turbia and Estero Molino flows in QTW-10 extends laterally northward and up-section, where it is crossed by the QTW-11 sampling traverse (Figure 3). Because of the southward facing paleotopography of this erosional surface, 20 Quebrada Turbia flows are preserved below the unconformity in the QTW-11 section. Units of the much younger Placeta San Pedro sequence sit above the unconformity and form the remainder of the canyon wall to its rim. Section QTW-11 is made up of 20 flows, all belonging to the Quebrada Turbia sequence, bounded on both the top and bottom by unconformities.

[10] Thickness of the Quebrada Turbia flows is commonly 1–2 m, although flows are thicker (3–7 m) toward the base of the QTW-10, where they show evidence of ponding. Some lavas are oxidized, especially along their top surfaces, but there is little or no visual indication of interior alteration of the flows. All of the Quebrada Turbia lavas are conformable and have intermingled breccia zones that show no evidence of intervening ash layers or paleosoil development. There is no evidence of faulting in this part of the volcano [*Singer et*

al., 1997], and flows are assumed to be in their original cooling positions.

3. Field Sampling

[11] The Tatara-San Pedro Complex is superbly exposed, allowing near-continuous sampling of eruptive sequences on a flow by flow basis [*Singer et al.*, 1997]. Samples for paleomagnetic, geochemical, and geochronological studies were taken from the same locations to minimize variations associated with cooling and compositional changes related to lava morphology. In particular, almost all samples were taken from within massive flow interiors to avoid the effects of reheating by subsequent flows and therefore any possible resetting of paleomagnetic directions. Erosional hiatuses and sedimentary units were mapped in detail in order to constrain any gaps in data. Further, care was taken to avoid the resampling of units; a mistake commonly made owing to the anastomosing nature of lava flows and the effects of topography on flow patterns.

[12] Between five and ten cores were collected from each lava flow for paleomagnetic analyses. Cores were drilled in the field with a portable gasoline-powered rock drill and were oriented in situ using an integrated sun compass and inclinometer. QTW-10 was sampled initially in 1992 with five samples collected per flow; these sites are reported by *Brown et al.* [1994]. The same flows were resampled in 1994 with eight cores drilled per site along with all flows in section QTW11. Geochronology samples were either collected as hand-samples at the same location as the paleomagnetic sites, or in some cases the paleomagnetic samples themselves were used for the argon work. Even though there is considerable outcrop on the west wall of Quebrada Turbia, it is not feasible to correlate specific flows from section QTW10 to QTW11. This is due to the steep nature of the canyon walls and the impossibility of walking out individual contacts.

4. Laboratory Methods

4.1. Paleomagnetic Methods

[13] Natural remanent magnetization (NRM) was measured using a Molspin spinner magnetometer in four positions at a spin period of 4 s. The majority of specimens were progressively step demagnetized using a Schonstedt GSD-1 alternating field (AF) demagnetizer and an ASC Model TD48 thermal specimen demagnetizer. AF demagnetization was performed in a series of steps from 2.5 to 80 mT, with some samples further demagnetized to 100 mT. At least one sample per flow was demagnetized in at least 12 steps providing detailed demagnetization information. Other samples were demagnetized with fewer steps. Selected samples were thermally demagnetized, using temperatures of 200°, 300°, 400°, 500°, 550°, 580 and 600°C. Primary directions were resolved through least squares analyses in most cases but single directions from one demagnetization level were used for some samples.

[14] Susceptibility was measured for each core on a Sapphire SI-2 susceptibility meter. Isothermal remanent magnetization behavior was investigated using an ASC Model IM-10 impulse magnetometer in fields up to 1.25 T. Other rock magnetic characteristics were measured at the Institute of Rock Magnetism at the University of Minnesota. These included coercivity spectrum analyses using a Micromag specimen analyzer in a peak field of 1.0 T and susceptibility-temperature information collected using a KLY-3 KappaBridge over temperature ranges from 20°C to 650°C.

[15] Geochemical samples, collected from the same flows as were sampled for paleomagnetism and geochronology, were analyzed for major and trace element compositions using standard XRF techniques [*Rhodes*, 1988]. Data on selected Quebrada Turbia samples are reported by *Dungan et al.* [2001], with complete data for each flow given by *Wulff* [1998].

4.2. The $^{40}Ar/^{39}Ar$ Methods

[16] Incremental heating experiments used a metal resistance furnace to degas 50 to 100 mg aliquots of holocrystalline groundmass in 5 to 15 steps between 600° and 1300°C. Seven experiments on three of the lava flows including QTW-10-3, QTW-10-8, and QTW10-10 are from *Singer and Pringle* [1996]. At the University of Wisconsin-Madison 21 additional incremental heating experiments were undertaken on subsamples of lavas QTW-10-2, QTW-10-3, QTW-10-5, QTW-11-3, QTW-11-5, QTW-11-11, QTW-11-16, QTW-11-17, and QTW-11-18. Procedures for preparing and irradiating samples, extracting gas from samples and fluence monitors, correcting for blanks, mass spectrometry, and estimating analytical uncertainties are detailed by *Singer et al.* [2002] and *Coe et al.* [2004].

[17] Ages are calculated relative to either the 28.34 Ma Taylor Creek (TCs) or 1.194 Ma Alder Creek (ACs) rhyolite sanidine that were used to monitor neutron fluence. As discussed by *Singer et al.* [2002] and *Coe et al.* [2004], the ages of these neutron fluence standards were adopted from their intercalibration to the 98.79 ± 0.96 Ma GA-1550 biotite standard [*Renne et al.*, 1998]. Where salient $^{40}Ar/^{39}Ar$ ages from the literature were not originally calculated relative to these standard values, these have been recalculated to allow direct comparison to our results. Samples were irradiated for one hour adjacent to TCs or ACs monitors in evacuated quartz vials at the Oregon State University Triga reactor in the Cadmium-Lined In-Core Irradiation Tube (CLICIT). Corrections for undesirable nucleogenic reactions on ^{40}K and ^{40}Ca are as follows: $[^{40}Ar/^{39}Ar]_K = 0.00086$; $[^{36}Ar/^{37}Ar]_{Ca} = 0.000264$; $[^{39}Ar/^{37}Ar]_{Ca} = 0.000673$ [*Wijbrans et al.*, 1995].

[18] Inverse-variance weighted mean plateau ages and uncertainties are calculated according to *Taylor* [1982]. Precision estimates for monitors, based on 6–7 measurements each suggest that the uncertainty in *J*, the neutron fluence parameter, was between 0.4 and 0.8% (±2σ); this uncertainty was propagated into the final plateau and isochron age for each analysis, but contributes <0.1% to the total uncertainty in these age estimates. Ages were calculated using the decay constants of *Steiger and Jäger* [1977] and are reported with ±2σ analytical uncertainties.

[19] Criteria used to determine whether an incremental heating experiment gave meaningful results were: (1) plateaus must be defined by at least three contiguous steps all concordant in age at the 95% confidence level and comprising >50% of the ^{39}Ar released, and (2) a well-defined isochron, calculated using the algorithm of

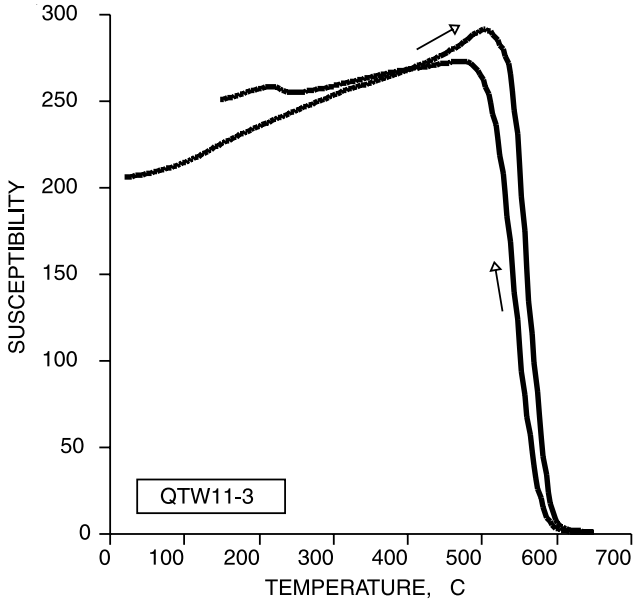

Figure 4. Susceptibility versus temperature plot for one sample from flow QTW11-3, demonstrating single-domain magnetite behavior.

York [1969] exists for the plateau points as defined by the F-variate statistic SUMS/(N-2). Because the isochron approach makes no assumption regarding the trapped component and combines estimates of analytical precision plus internal disturbance of the sample (scatter about the isochron), the isochron ages are preferred over the weighted mean plateau ages. Where multiple subsamples were measured from a lava, the weighted mean of the individual isochrons gives our best estimate of the age of the flow [*Singer et al.*, 2002; *Coe et al.*, 2004].

5. Results

5.1. Rock Magnetism and Demagnetization Behavior

[20] Samples from the Quebrada Turbia lavas, in both the medial and distal sections, demonstrate similar rock magnetic behavior. Temperature dependent variations in susceptibility indicate that samples are dominated by magnetic carriers with Curie temperatures in the range of 550°–580°C (Figure 4). Although slight differences in the temperature of maximum susceptibility were observed, the Curie-temperature curves suggest that low titanium-titanomagnetite or magnetite is the common carrier in the sampled lavas. Coercivity measurements, conducted on at least one sample per flow, confirm these conclusions. The ratio of saturation remanence to saturation magnetization varies from 0.1 to 0.3 for all samples, while the ratio of coercive force to coercivity remanence yields values from 1.8 to 3.9. When these two ratios are plotted against each other [after *Day et al.*, 1977] all points fall within the pseudo-single domain space for magnetite (Figure 5). Field saturation levels on samples were reached by 0.1–0.3 T, again indicating magnetite as the primary oxide present.

[21] Quebrada Turbia sequence flows from section QTW-10 (sites 2–11) exhibit a range of alternating field demagnetization behaviors. Cores from the basal flow (QTW-10-2) have a normal low-coercivity viscous overprint that is removed by 20 mT, at which point a high-coercivity primary component is progressively demagnetized (Figure 6a). Transitional flows QTW-10-3 to 11 possess a consistent overprint, with initial positive inclinations and often westerly declinations. In some instances a primary component is obtained by levels of 20 mT (Figure 6b). In other cases the overprint and primary components overlap, and alternating fields of 50 mT or more are required to isolate the primary component (Figure 6c). Occasionally AF demagnetization was unable to completely remove the overprint; such samples were excluded from site mean calculations. The observed overprint with a down and southwest to west direction is not the expected overprint of a normal field as seen in QTW10-2 (Figure 6a). Thermal studies on companion samples revealed similar demagnetization behavior and directions, but proved to be no better at isolating primary components (Figure 6d).

[22] Samples from the distal section (QTW-11) demonstrate simpler demagnetization behavior with south-southwesterly declinations and negative intermediate inclinations (Figures 6e, 6f, and 6g). Many samples displayed no overprints and were dominated by single component, high-coercivity remanences (Figure 6g). Other samples showed low-coercivity overprints but these were removed by 20–40 mT, after which primary vectors showed straight-line decay to the origin (Figure 6f).

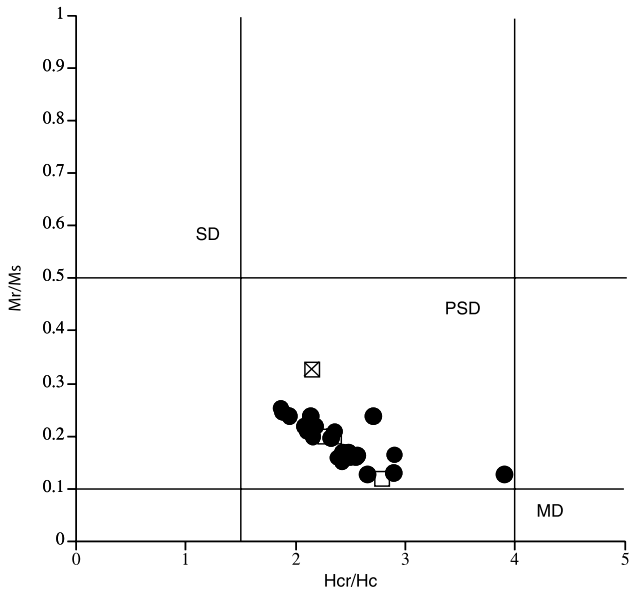

Figure 5. Magnetic domain classification plot of selected samples from all sampled Quebrada Turbia sequence flows in sections QTW-10 and QTW-11 (method after *Day et al.* [1977]). Data are plotted as remanence ratio (Mr/Ms) versus coercivity ratio (Hcr/Hc). All transitional (solid circles), reverse polarity (box with "x") and normal polarity (open boxes) flows fall within the pseudo-single-domain (PSD) field. Abbreviations are as follows: Mr, remanent saturation magnetization; Ms, saturation magnetization; Hc, coercive force required to reduce Mr to zero; Hcr, coercivity of remanence, MD, multidomain space, SD, single domain space.

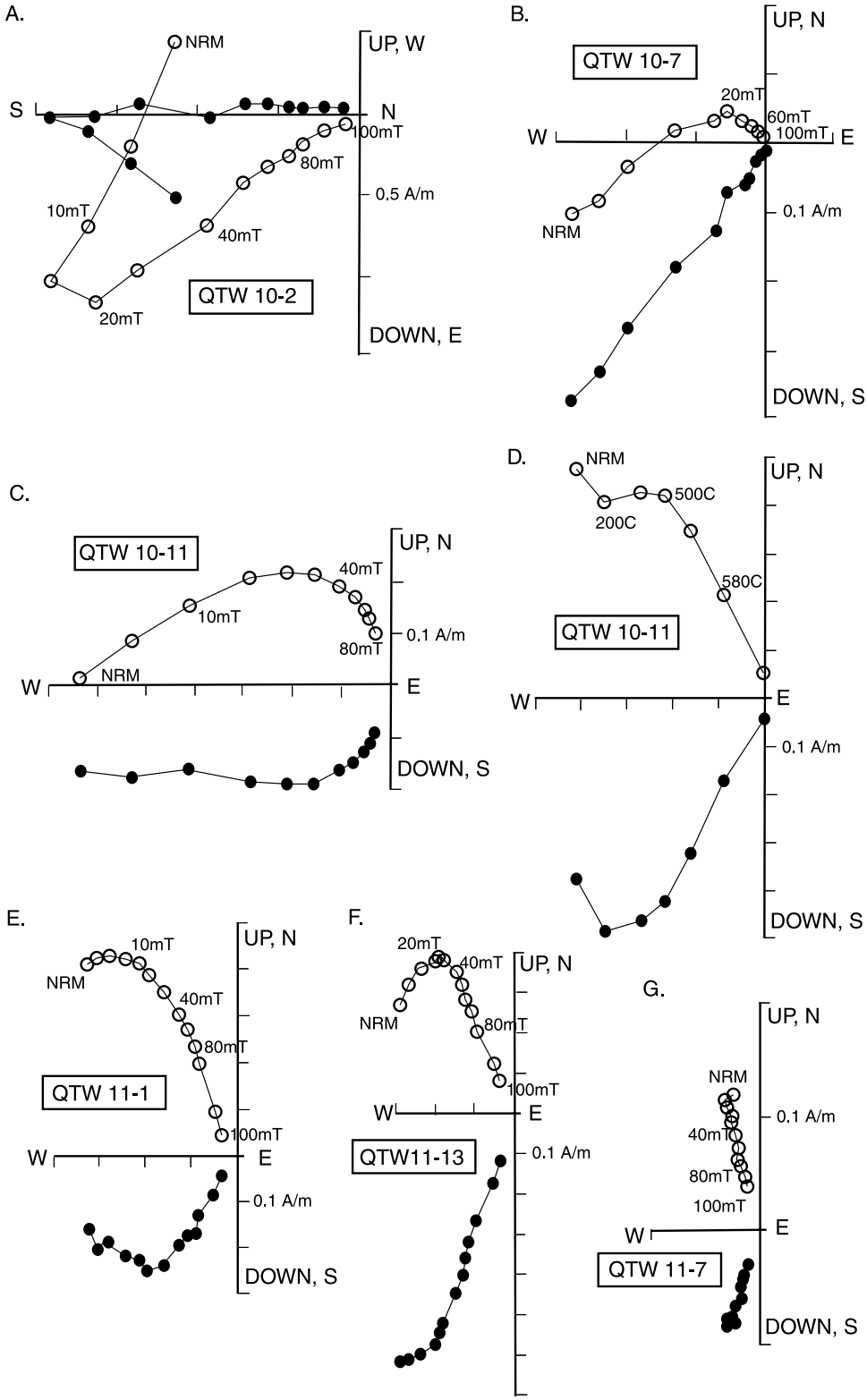

Figure 6. Vector endpoint diagrams demonstrating field behavior during progressive demagnetization for the following: (a) alternating field demagnetization of QTS reversed flow in section QTW-10, below the first transitional flows; (b) alternating field demagnetization of sample from transitional site in QTW-10 section; (c and d) alternating field and thermal demagnetization behavior from companion specimens from transitional site in QTW-10 section; (e–g), alternating field demagnetization of samples from transitional flows in section QTW-11. NRM is natural remanent magnetization; open circles are projections onto the vertical plane; solid circles are projections onto the horizontal plane.

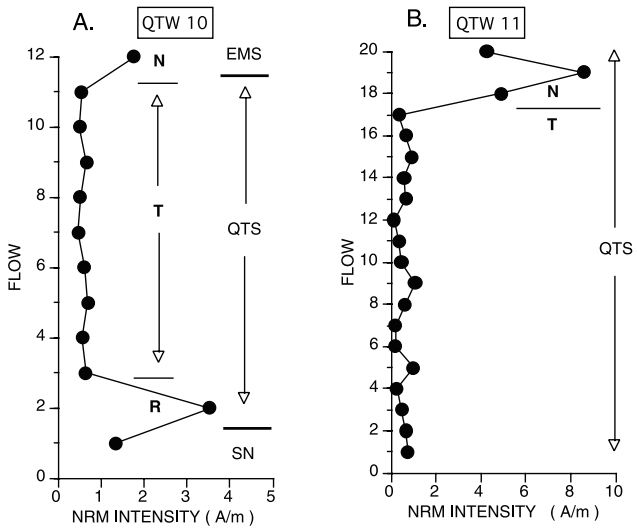

Figure 7. Site mean NRM intensity values for flows in sections (a) QTW-10 and (b) QTW-11. Labels are as follows: N, normal; T, transitional; R, reversed; Qmsn, Sin Nombre lavas of the Munoz sequence; Qqt, Quebrada Turbia lavas; Qt, Volcan Tatara lavas. See Figures 2 and 3 for stratigraphy.

[23] Natural remanent magnetization (NRM) intensities averaged for each flow are plotted in Figure 7. In section QTW-10 NRM levels drop close to an order of magnitude for the Qqt samples as compared to the basal Munoz flow and the one reverse polarity Qqt flow (Figure 7). Above the unconformity separating Quebrada Turbia and Estero Molino flows, intensity levels again rise by an order of magnitude. Similar, low-intensity values are observed for the first 17 flows of the distal section (Figure 7). Between flows QTW-11-17 and QTW-11-18, intensity levels increase by an order of magnitude for Qqt normal polarity lows at the top of the section. Magnetic susceptibility values are similar for all the flows within the Quebrada Turbia sequence. Mean susceptibility for the 26 transitional flows is 1.87×10^{-2} SI, while the four full polarity flows average 1.70×10^{-2} SI.

[24] The similarity in magnetic mineralogy, magnetic susceptibility, and constant whole rock geochemistry of the Qqt flows precludes that these dramatic changes in intensity are a purely mineralogical phenomenon. The susceptibility-temperature and coercivity spectrum analyses discussed above indicate that the dominant magnetic carrier is consistently pseudo-single-domain magnetite for the flows immediately before and after the changes in intensity as well as for the low intensity samples (Figure 5).

5.2. Section QTW-10 Paleomagnetic Results

[25] Two reverse polarity flows lie at the base of QTW-10, the basal Sin Nombre lava of the Munoz sequence (QTW-10-1) followed by an ash layer and then the lowermost Quebrada Turbia flow (QTW-10-2). Both have distinctive reverse polarity directions and do not overlap at the 95% level (Table 1). Nine transitional units (site 3-11) follow, and are then bounded by an unconformity separating the Quebrada Turbia and Estero Molino sequences. The bottom two flows have positive inclinations and south-southwesterly declinations. The change from reverse polarity (QTW-10-1 and QTW-10-2) to transitional (QTW-10-3-11) field directions is abrupt, with declination remaining fixed in a southerly attitude but inclination switching from positive to steeply negative (Figure 8a and Table 1). For the overlying Quebrada Turbia flows, directions show only small variations in inclination and declination. Flows above the unconformity are all normal in polarity, as shown by QTW-10-12 but much younger in age. Note that site data for section QTW-10 differ somewhat from those published earlier [*Brown et al.*, 1994] owing to complete resampling of the section and more extensive demagnetization procedures.

5.3. Section QTW-11 Paleomagnetic Results

[26] Reverse polarity lavas are not present in section QTW-11, but 17 transitional units and 3 overlying normal polarity lavas are preserved. The site directional averages are relatively consistent for the transitional flows of QTW-11, and they match those observed in QTW-10 (Figure 8b and Table 1). For the first 17 flows, directions are transitional with declinations consistently south-southwesterly and inclinations negative and intermediate. Collectively, these 17 sites form a tight cluster of directions ($\alpha_{95} = 1.80°$). Between QTW-11-17 and QTW-11-18, declination values change abruptly to the north, indicating a switch to normal polarity. Inclination values remain similar, at $-60°$, but declinations migrate $\sim 160°$ to the north-northeast.

5.4. The $^{40}Ar/^{39}Ar$ Results

[27] Twenty-five of the 28 incremental heating experiments yielded age spectra with more than 70% of the gas defining the age plateaus (Table 2 and Appendix A, which is available as auxiliary material[1]). Most of the small percentage of discordant steps yielded apparent ages slightly lower than the plateau ages, suggesting that a limited amount of argon loss may have occurred in some lavas (Figures 9 and 10). Exceptions include the experiments on lavas QTW-11-3 and QTW-10-8 which produced weakly saddle-shaped spectra that, notwithstanding, yield age plateaus and isochrons satisfying the criteria above (Table 2; Figures 9 and 10). No isochron yielded $^{40}Ar/^{36}Ar_i$ values significantly different than 295.5 indicating that excess argon is not present in detectable levels that might bias the results (Figures 9 and 10). The 11 isochron ages span the southerly (QTW-10-2, QTW-10-3, QTW-10-5, QTW-10-8, and QTW-10-10) and northerly sections (QTW-11-3, QTW-11-5, QTW-11-11, and QTW-11-16, QTW-11-17, and QTW-11-18), including 9 of the transitionally magnetized lava flow sites (Figures 9 and 10). Three experiments on reversely magnetized flow QTW-10-2 gave a combined isochron age of 811.0 ± 30.0 ka (Table 2 and Figure 9). The combined isochron ages of the nine transitionally magnetized flows are between 801.0 ± 12.0 ka and 790.2 ± 6.1 ka and at face value are not in stratigraphic order (Figure 3), yet at the 95% confidence level none of these isochrons is distinguishable from one another (Table 2). Thus we take the inverse-variance weighted mean of the nine isochrons, 791.7 ± 3.0 ka (MSWD) = 0.38), as our best estimate for the time since eruption of these lavas during a portion of the Matuyama-Brunhes reversal. Three experi-

[1] Auxiliary material is available at ftp://ftp.agu.org/apend/jb/2004JB003007.

Table 1. Site Mean Paleomagnetic Data for the Lower Parts of Sections QTW-10 and QTW-11[a]

Site	*N*/*n*	Sequence	Weighted Mean Age, ka	Mean Magnetization Direction					Virtual Geomagnetic Pole	
				Declination	Inclination	*k*	α_{95}	P	Latitude	Longitude
				Quebrada Turbia West, Section 10						
12[b]	5/5	EMS	330 ± 40[c]	324.4	−54.8	259	6.7	N	61.3	189.7
11[b]	8/8	QTS		221.3	−41.8	74	6.5	T	−18.4	148.4
10	7/8	QTS	790.1 ± 12.6	200.3	−43.7	55	8.2	T	−25.6	129.3
9	8/8	QTS		229.4	−44.5	22	12.0	T	−12.3	153.3
8	8/8	QTS	790.8 ± 6.7	214.5	−43.4	44	8.5	T	−20.6	142.1
7	8/8	QTS		209.2	−34.9	50	7.9	T	−28.3	140.5
6	7/7	QTS		203.4	−41.7	146	5.0	T	−26.1	132.8
5	8/8	QTS	790.3 ± 8.6	216.2	−45.2	46	8.3	T	−18.6	142.8
4	7/7	QTS		244.9	−37.7	97	6.2	T	−6.3	167.2
3	8/8	QTS	790.2 ± 6.1	213.4	−58.3	37	9.2	T	−8.9	134.7
2[b]	7/8	QTS	811.0 ± 30.0	186.4	35.9	55	8.2	R	−72.9	129.9
1[b]	8/8	SNS	975 ± 176[c]	205.2	68.2	393	2.8	R	−66.5	247.3
				Quebrada Turbia West, Section 11						
20	7/8	QTS		356.8	−55.6	521	2.3	N	87.4	194.6
19	8/8	QTS		352.1	−62.3	1041	2.1	N	80.2	146.2
18	7/8	QTS	784.1 ± 9.9	11.0	−61.0	311	3.2	N	79.6	58.0
17	7/8	QTS	801.0 ± 12.0	214.4	−57.0	82	6.2	T	−9.8	136.0
16	8/8	QTS	791.3 ± 7.9	208.4	−40.8	191	3.8	T	−24.8	137.8
15	8/8	QTS		200.3	−35.4	98	5.3	T	−31.2	131.4
14	7/8	QTS		201.4	−39.1	643	2.2	T	−28.4	131.6
13	7/8	QTS		199.9	−37.5	489	2.3	T	−30.0	130.5
12	7/8	QTS		201.7	−40.0	171	4.3	T	−27.8	131.7
11	6/8	QTS	792.9 ± 17.1	212.9	−35.8	269	3.7	T	−26.1	143.7
10	7/8	QTS		195.7	−30.2	130	5.4	T	−35.7	127.7
9	8/8	QTS		198.5	−38.1	259	3.2	T	−29.3	128.7
8	8/8	QTS		207.8	−40.8	31	9.4	T	−25.1	137.2
7	8/8	QTS		200.2	−49.4	544	2.2	T	−21.1	127.6
6	8/8	QTS		197.8	−49.5	256	3.2	T	−21.6	125.5
5	8/8	QTS	793.8 ± 9.8	197.4	−44.5	210	3.6	T	−25.7	126.3
4	8/8	QTS		191.7	.49.0	168	4.0	T	−23.2	120.0
3	8/8	QTS	795.0 ± 21.0	202.7	−47.7	85	5.6	T	−21.8	130.3
2	7/8	QTS		204.7	−48.6	313	3.2	T	−20.5	131.9
1	9/9	QTS		210.3	−53.9	154	3.9	T	−14.0	134.3

[a] *N*/*n* is the number of samples used in the mean calculations to number of samples collected; QTS, Quebrada Turbia Sequence; EMS, Estero Molino Sequence; SNS, Sin Nombre Sequence; *k* and α_{95} are statistical parameters from *Fisher* [1953]. For polarity (P), N is normal, T is transitional, R is reversed. Declination, inclination, α_{95}, latitude, and longitude are all in degrees.
[b] Ash layers are found between the lowermost two flows (QTW-10-1 and QTW-10-2) and uppermost two flows (QTW-10-11 and QTW-10-12).
[c] Radioisotopic age determinations are from *Singer et al.* [1997] and *Singer and Pringle* [1996].

ments on normally magnetized flow QTW-11-18 gave a combined isochron age of 784.1 ± 9.9 ka, indicating eruption in the very earliest portion of the Brunhes Chron (Table 2 and Figure 10).

5.5. Correlation of Sections

[28] The supporting geochemical data, detailed radioisotopic dating, and careful field mapping combine to provide a well-constrained transitional record. The movement from reverse polarity to transitional virtual geomagnetic poles (VGPs) is recorded in the base lavas of QTW-10, without any evidence of an unconformity between these flows (QTW-10-2 and QTW-10-3). Similarly, the change from transitional to normal polarity VGPs (QTW-11-17 and QTW-11-18) is recorded in consecutive lavas without any discernible temporal hiatus. Furthermore, within the transitional packages of each section there are no indications of appreciable breaks in lava production. Together, the two sampled sections appear to span the transitional event, with some overlap between the 26 transitional flows. The two major unconformities which bracket these lavas act as marker horizons that can be traced directly along the west wall of the canyon, linking the two sections (Figure 3).

[29] The similarity in whole rock geochemical profiles between the two sections strengthens the direct association between the medial and distal sections [*Dungan et al.*, 2001]. The Quebrada Turbia lava flows of QTW-10 are defined as basaltic andesites, but two eruptive packages can be distinguished geochemically [*Dungan et al.*, 2001]. Major element abundances (e.g., CaO and MgO) subdivide the QTW-10 section into package QTW-10-1 to 5, intermediate flow QTW-10-6, and package QTW-10-7 to 11 (Figure 11a). Flows in section QTW-11, which are also classified as basaltic andesites, have major element concentrations that match those of QTW-10-7 to 11 (Figure 11b). The chemistry in QTW-11 remains essentially invariant for all transitional flows and the first two normal units. This correspondence in element abundances between the sections as seen in Figure 11 as well as more detailed geochemical comparisons [*Dungan et al.*, 2001] indicates that they were comagmatic and that flows QTW-10-7 to 11 are the equivalents of those which lie at the base of QTW-11. The upper three flows in QTW-11 (18 to 20) have relatively larger fluctuations in geochemistry than seen in the flows directly below, but they still indicate strong geochemical affinities to the other QTW flows *Dungan et al.*, 2001, Figure 11].

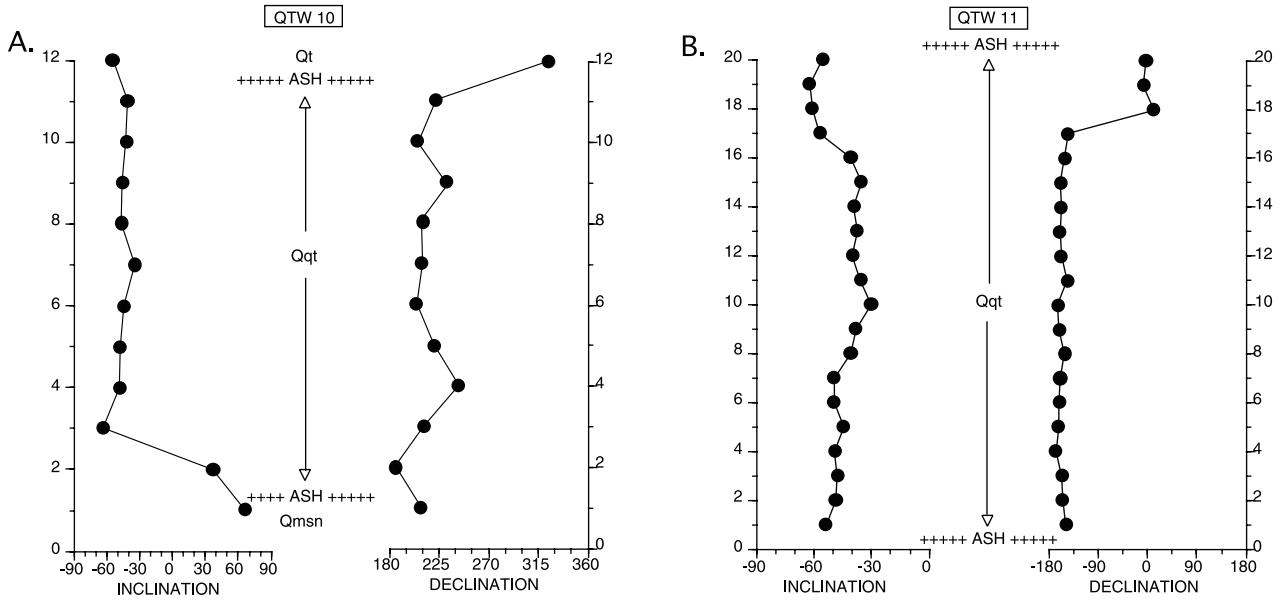

Figure 8. Paleomagnetic inclination and declination site means for the Quebrada Turbia lavas. (a) Section QTW-10 from flow 1 through flow 12. Note the presence of ash layers between the lowermost two flows (QTW-10-1 and QTW-10-2) and between the uppermost two flows (QTW-10-11 and QTW-10-12). The ash layers also mark temporal hiatuses. (b) Section QTW-11 from flow 1 through flow 20. Note there are ash layers below flow 1 and above flow 20. Sequence nomenclature as in Figure 7.

[30] The two eruptive packages identified in the QTW flows, along with the minor variations seen in the upper package, represent subcyclic magma generation and minor differentiation of a common parent magma [*Dungan et al.*, 2001]. Although there is no specific evidence from the geochemistry on the timing of eruptive phases, if the period between eruptions had been relatively long or if flows had been discharged in discrete batches, more extreme geochemical evolution would be expected owing to magma chamber differentiation processes. The intermingled breccia zones of flows and the lack of any interflow paleosoils in either section corroborate these geochemical data, suggesting relatively rapid eruption.

6. Discussion

6.1. Age and Significance of the Transitional Event

[31] The agreement between K-Ar ages of 768 ± 16 and 763 ± 28 ka (2σ) for transitionally magnetized lavas QTW-10-3 and QTW-10-10 (Figure 3), respectively, and both $^{40}Ar/^{39}Ar$ [*Baksi et al.*, 1992; *Spell and McDougall*, 1992; *Izett and Obradovich*, 1994] and astrochronologic [*Shackleton et al.*, 1990] ages of ~780 ka for the Matuyama-Brunhes reversal, led *Brown et al.* [1994] to conclude that these lavas recorded part of the M-B reversal process. Later $^{40}Ar/^{39}Ar$ dating of these two lavas, plus two other transitional lavas QTW-10-8 and QTW-11-17 (Figure 3) by *Singer and Pringle* [1996] gave a mean age of 781.3 ± 4.7 ka for this lava sequence thereby reinforcing the conclusion that they record the Matuyama-Brunhes reversal. However, it is critical to note that the $^{40}Ar/^{39}Ar$ ages originally reported by *Singer and Pringle* [1996] were calculated relative to a 27.92 Ma age for sanidine of the Taylor Creek Rhyolite that was used as a secondary standard to monitor the neutron fluence [*Duffield and Dalrymple*, 1990]. More recently, the intercalibration by *Renne et al.* [1998] of several standards against the primary GA-1550 biotite standard indicates that the Taylor Creek Rhyolite sanidine is 28.34 Ma, which is 1.015% older than the value used by *Singer and Pringle* [1996]. Recalculation of the ages determined by *Singer and Pringle* [1996] gives a mean for the transitional lavas in Quebrada Turbia of 793.0 ± 4.7 ka. The new $^{40}Ar/^{39}Ar$ results presented here, combined with the recalculated ages from *Singer and Pringle* [1996], give a weighted mean age for nine of the transitionally magnetized lavas of 791.7 ± 3.0 ka that is precise to better than 0.4% on the basis of analytical uncertainty alone.

[32] The age of 791.7 ± 3.0 ka for the recorded transitional event is at odds with both $^{40}Ar/^{39}Ar$ dating and the best astrochronologic constraints on the age of the M-B reversal. The most detailed recording of the M-B reversal by lava flows is found in the Haleakala caldera atop the island of Maui. Using procedures and standards identical to those described here, *Coe et al.* [2004] determined $^{40}Ar/^{39}Ar$ ages from 6 of the 24 lavas that record the M-B reversal on Maui that are indistinguishable from one another and give a weighted mean age of 775.6 ± 1.9 ka (2σ, analytical uncertainty). Because the Maui lavas were dated using the same methods and standards in the same laboratories used in the present study, systematic uncertainties associated with the ^{40}K decay constant and standard intercalibrations may be ignored and these results can be compared directly using the analytical uncertainty alone. Thus, at the 95% confidence level, the age of 775.6 ± 1.9 ka of the Maui lavas is younger by 16 ± 4 kyr than the Quebrada Turbia sequence. The $^{40}Ar/^{39}Ar$ age of the transition recorded by the Maui lavas does, however, agree remarkably well with the astrochronologic age for the Matuyama-Brunhes reversal [*Coe et al.*, 2004]. *Tauxe et al.* [1996] synthesized results from 18 marine sediment core records from around the

Table 2. Summary of $^{40}Ar/^{39}Ar$ Incremental Heating Experiments, Quebrada Turbia, Chile

Sample and Experiment	Weight, mg	K/Ca Total	Total Fusion Age ± 2σ, ka	Increments Used, °C	Age Spectrum				Isochron Analysis		
					^{39}Ar, %	Age ± 2σ, ka	MSWD	*N*	MSWD	$^{40}Ar/^{36}Ar_i$ ± 2σ	Age ± 2σ, ka
QTW-11-18											
UW18G58[a]	100	0.520	780 ± 11	900–1275	100.0	779.7 ± 9.4	0.49	4 of 4	0.74	295.5 ± 2.6	779.6 ± 14.6
UW18G59[a]	100	0.498	784 ± 11	850–1280	100.0	784.1 ± 12.9	0.64	5 of 5	0.45	294.1 ± 2.5	791.2 ± 16.9
UW18G60[a]	100	0.482	782 ± 14	850–1300	100.0	781.2 ± 13.0	0.35	5 of 5	0.46	295.3 ± 3.4	782.4 ± 22.8
Weighted mean isochron								14 of 14	0.55		784.1 ± 9.9
QTW-11-17											
UW18G54[a]	100	0.365	796 ± 20	800–1215	100.0	798.5 ± 14.3	0.05	7 of 7	0.04	295.3 ± 1.3	801.8 ± 23.8
UW18G55[a]	100	0.367	777 ± 17	950–1155	89.0	798.1 ± 11.2	0.52	4 of 5	0.76	295.8 ± 2.1	795.9 ± 20.9
UW18G56[a]	100	0.354	797 ± 19	875–1275	100.0	799.2 ± 12.2	0.23	6 of 6	0.16	295.0 ± 1.4	805.1 ± 20.5
Weighted mean isochron								17 of 18	0.20		801.0 ± 12.0
QTW-11-16											
UW01A10[b]	77	0.326	788 ± 19	880–1250	84.2	782.9 ± 15.4	1.02	9 of 15	1.11	294.2 ± 4.3	787.3 ± 21.7
UW10E98[a]	100	0.376	788 ± 8	650–1400	100.0	788.2 ± 5.6	1.20	8 of 8	1.20	294.3 ± 2.2	791.9 ± 8.5
Weighted mean Isochron								17 of 22	0.16		791.3 ± 7.9
QTW-11-11											
UW01A09[b]	81	0.388	769 ± 11	600–1040	82.7	793.0 ± 9.3	0.90	9 of 13	1.02	295.5 ± 4.5	792.9 ± 17.1
QTW-11-5											
UW10E97[a]	100	0.425	784 ± 8	775–1350	100.0	788.2 ± 7.3	1.47	7 of 7	1.24	292.8 ± 3.8	794.9 ± 11.5
UW10D116[a]	100	0.454	780 ± 8	800–1175	80.8	783.6 ± 8.3	2.11	4 of 5	2.87	298.4 ± 13.3	778.1 ± 26.8
UW01A08[b]	80	0.379	765 ± 13	600–1050	86.3	790.4 ± 13.5	1.58	9 of 12	1.54	291.5 ± 7.3	802.2 ± 25.4
Weighted mean isochron								20 of 24	0.92		793.8 ± 9.8
QTW-11-3											
UW01A07[b]	76	0.429	796 ± 18	930–1250	78.3	784.5 ± 17.9	1.23	8 of 11	1.03	291.9 ± 4.7	800.0 ± 25.8
UW01A06[b]	80	0.397	760 ± 11	930–1070	57.6	784.7 ± 9.0	0.16	4 of 12	0.23	295.0 ± 11.7	786.3 ± 36.6
Weighted mean isochron								12 of 23	0.37		795.0 ± 21.0
QTW-10-10											
95GEA04[c]	59	0.652	792 ± 6	840–1100	76.9	792.7 ± 6.4	0.36	8 of 11	0.42	296.7 ± 5.4	790.1 ± 12.6
QTW-10-8											
95GEB54[c]	57	0.459	798 ± 12	880–1035	71.9	797.2 ± 12.0	0.65	6 of 10	0.71	289.9 ± 20.2	804.8 ± 29.4
95GEB53[c]	63	0.459	752 ± 8	850–970	83.7	785.4 ± 7.8	0.37	5 of 7	0.40	291.2 ± 9.8	790.0 ± 19.2
95GEA04[c]	59	0.419	792 ± 6	865 1250	86.2	788.8 ± 6.8	0.66	8 of 9	0.69	294.4 ± 2.8	790.0 ± 7.4
Weighted mean isochron								19 of 26	0.48		790.8 ± 6.7
QTW-10-5											
UW10E96[a]	100	0.838	785 ± 6	800–1150	76.6	789.3 ± 4.4	0.92	5 of 6	1.21	296.4 ± 6.6	788.0 ± 11.1
UW10E95[a]	100	0.735	789 ± 7	760–1300	94.1	794.8 ± 5.5	1.03	6 of 7	1.27	295.9 ± 5.7	793.9 ± 13.8
Weighted mean isochron								11 of 13	0.44		790.3 ± 8.6
QTW-10-3											
UW01A02[b]	79	0.684	762 ± 16	830–1250	100.0	765.0 ± 14.1	0.36	10 of 10	0.30	292.6 ± 6.2	772.8 ± 21.9
UW01A01[b]	78	0.668	756 ± 21	850–1250	97.8	772.3 ± 17.5	0.53	10 of 11	0.30	288.3 ± 9.2	790.4 ± 28.7
95GEB70[c]	53	1.163	799 ± 8	805–950	56.0	791.6 ± 7.0	0.54	7 of 13	0.69	296.9 ± 9.8	790.1 ± 12.2
95GE00B[c]	50	1.070	775 ± 12	850–1080	62.9	774.5 ± 9.6	0.86	6 of 10	0.81	299.8 ± 9.2	766.9 ± 18.4
95GEB71[c]	55	1.205	797 ± 7	800–1200	93.1	797.9 ± 7.0	1.45	11 of 13	1.74	295.8 ± 4.2	797.6 ± 8.4
Weighted mean isochron								44 of 57	3.00		790.2 ± 6.1
QTW-10-2											
UW18G50[a]	100	0.397	804 ± 18	750–1250	100.0	802.4 ± 13.2	0.77	6 of 6	0.94	294.8 ± 4.2	808.3 ± 39.5
UW18G52[a]	100	0.375	797 ± 22	875–1250	100.0	796.7 ± 20.4	0.07	5 of 5	0.03	296.8 ± 5.7	780.9 ± 72.6
UW18G53[a]	100	0.378	816 ± 20	800–1250	100.0	820.2 ± 17.2	0.89	6 of 6	1.01	293.8 ± 5.5	837.3 ± 58.7
Weighted mean isochron								17 of 17	0.75		811.0 ± 30.0

[a]Ages are calculated relative to 28.34 Ma Talyor Creek Rhyolite sanidine [*Renne et al.*, 1998].
[b]Ages are calculated relative to 1.194 Ma Alder Creek Rhyolite sanidine [*Renne et al.*, 1998].
[c]Data are from *Singer and Pringle* [1996].

globe that give astronomical ages for the M-B reversal of between 784.2 ± 19.4 ka and 769.9 ± 3.8 ka, with a mean of 777.9 ± 3.6 ka (2σ). The best astronomical age for the M-B reversal is thus 14 ± 2 kyr younger than the transition recorded in Quebrada Turbia. Moreover, *Clement* [2004] has shown that the duration of the M-B reversal as recorded in 17 sediment cores is unlikely to have exceeded 7 kyr. It seems therefore unlikely that the Quebrada Turbia lavas record the polarity change associated with the M-B reversal. We next explore the significance of this finding.

[33] High resolution measurements of marine sediment cores have revealed significant variability of the magnetic

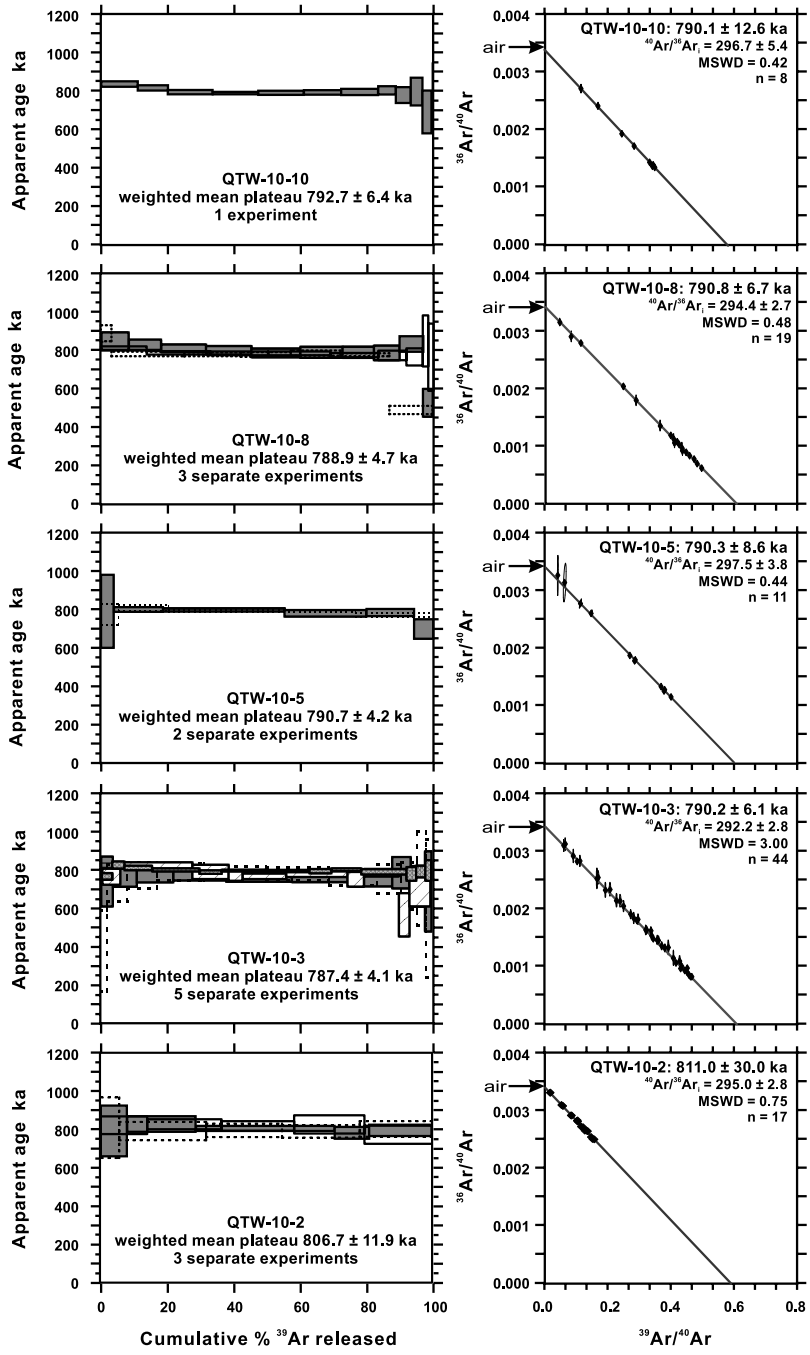

Figure 9. Age spectra and isotope correlation diagrams for five samples from section QTW-10. The preferred isochron age of each lava is the weighted mean of isochrons calculated from multiple subsamples. The $^{40}Ar/^{36}Ar_i$ values for each lava are those of a combined isochron calculated by normalizing J values for individual experiments; these are shown only to illustrate that all lavas contain a trapped component indistinguishable from atmospheric argon.

field during the 25 kyr leading up to the M-B reversal [*Schneider et al.*, 1992; *Kent and Schneider*, 1995; *Hartl and Tauxe*, 1996; *Channell and Kleiven*, 2000]. *Hartl and Tauxe* [1996] show that a prominent feature common to 12 cores from around the world is a pair of relative paleointensity lows centered upon: 1. the M-B reversal, and 2. a period of time about 15 kyr prior to the reversal. This same pattern of dual paleointensity lows have been astronomically dated at 793 and 775 ka, with the latter event corresponding to a relatively abrupt reverse-to-normal directional change in VGPs, from the analysis by *Channell and Kleiven* [2000] of sediment that accumulated at an exceptionally high rate of 13 cm/kyr at ODP site 983. Given the radioisotopic age from Maui and these astrochronologic constraints, the precursor event to the M-B reversal occurred about 793 ka—in other words it is temporally identical to the $^{40}Ar/^{39}Ar$ age of the transitionally magnetized lavas in Quebrada Turbia. Contrary to conclusions

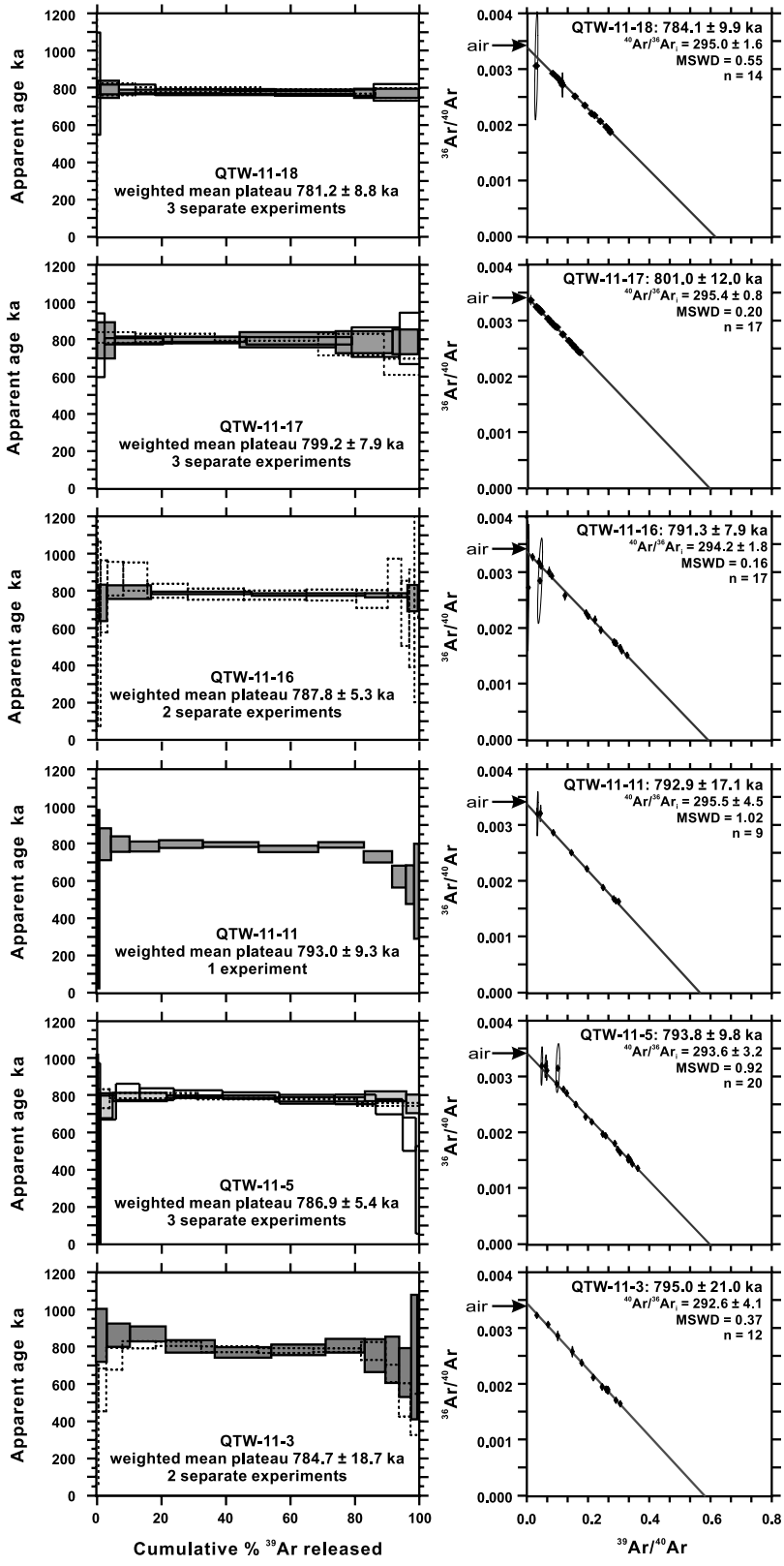

Figure 10. Age spectra and isotope correlation diagrams for six samples from section QTW-11. Isochrons and $^{40}Ar/^{36}Ar_i$ values calculated as in Figure 9.

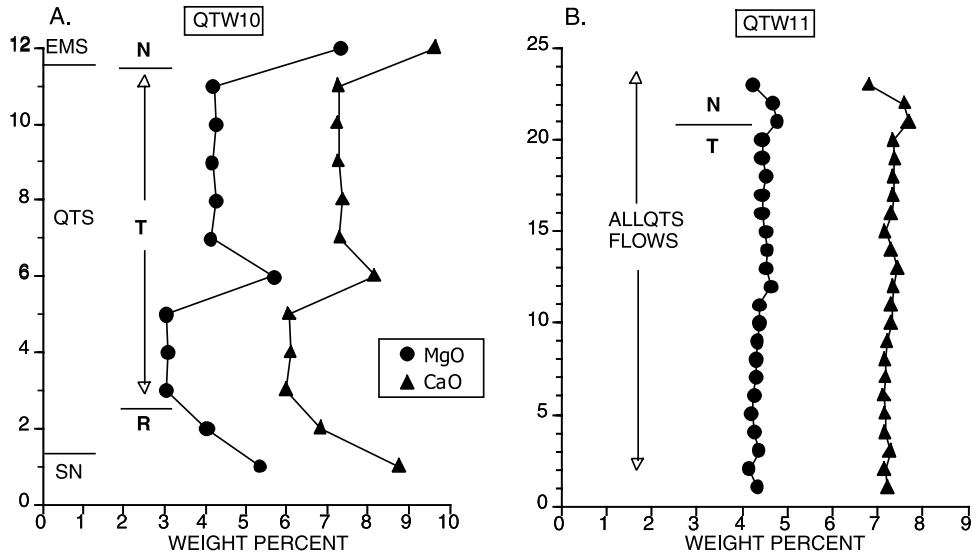

Figure 11. Major element abundance data using MgO (circles) and CaO (triangles) for sections (a) QTW-10 and (b) QTW-11. MgO and CaO abundances for flows QTW-10-7-11 and QTW11-1-23 are nearly identical, suggesting their comagmatic nature. Vertical axes are flows by number, as in Table 1. Heavy solid lines indicate erosional breaks; light solid lines indicate changes in polarity. Rock unit designations and polarity indications as in Figure 7. Geochemical data from *Wulff* [1998].

reached previously by *Brown et al.* [1994] and *Singer and Pringle* [1996], we propose that the lavas in Quebrada Turbia may not record the polarity change associated with the M-B reversal, but rather provide a terrestrial record of directional change that accompanied the low field intensity during an event precursory to the final, complete reversal of the field. Moreover, the $^{40}Ar/^{39}Ar$ age of 791.7 ± 3.0 ka gives a precise calendar age for this event.

[34] Our findings raise the question of whether or not other lava flow sequences thought to record the M-B reversal on the basis of K-Ar or $^{40}Ar/^{39}Ar$ dating may instead record the precursor event. For example, the weighted mean $^{40}Ar/^{39}Ar$ age of three of four transitionally magnetized lavas on La Palma thought to record the M-B reversal was determined in the same lab using the same standards as the present study and is 798.4 ± 6.3 ka [*Singer et al.*, 2002]. A single transitionally magnetized lava on Tahiti thought to record the M-B reversal was dated by *Singer and Pringle* [1996] at 784.6 ± 14.2 ka, but when recalculated using the standard ages of the present study its age becomes 796.4 ± 14.2 ka. Neither the age of the three flows at La Palma, nor the single less precise age from Tahiti are consistent with these lava sequences preserving records of the M-B reversal. Further dating underway on the Tahitian lavas is needed to confirm this finding. If this interpretation of the $^{40}Ar/^{39}Ar$ data is correct, there is only one $^{40}Ar/^{39}Ar$ dated lava sequence at Maui that records the M-B reversal [*Coe et al.*, 2004], and three others in Chile, La Palma, and Tahiti that may reflect field behavior during the precursor event. If our interpretation is correct, these lava records vividly emphasize the highly fragmentary nature of the paleomagnetic record and its inability to give us a comprehensive picture of the reversal process [*Coe and Glen*, 2004].

6.2. Observed Transitional Behavior

[35] The reversal as seen at Tatara-San Pedro is characterized by predominance of one transitional direction. Virtual geomagnetic poles for lavas from both section QTW-10 and QTW-11 cluster over Australasia (Figure 12 and Table 1). As recorded in these data, the observed transition is characterized by a jump from reversed polarity (QTW-10-2) to the stationary transitional grouping (QTW-10-3-11 and QTW-11-1-17). There are no extraordinary directional changes in the transitional data, with all VGPs lying within the subequatorial cluster (6 to 36°S) and thus no transitional

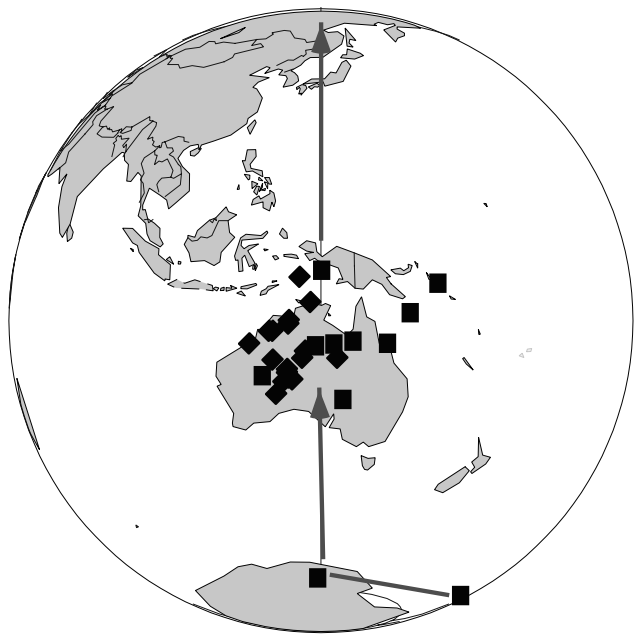

Figure 12. Virtual geomagnetic poles for reversed and transitional sites of sections QTW-10 (solid squares) and QTW-11 (shaded diamonds). Three normal poles from QTW-11 are not shown owing to orientation of the global projection.

poles appearing in the Northern Hemisphere. The mean pole position for the 26 transitional flows is 22.7°S, 135.7°E, with a circle of confidence of 4.2°. This population of poles is coincident with one of two transitional pole clusters introduced by *Hoffman* [1992] and used to support the presence of inclined dipolar fields during the reversal process.

[36] It is tempting to present the sequence measured in Quebrada Turbia as a complete record of the Matuyama/Brunhes reversal, as was done by *Brown et al.* [1994]. As discussed above, $^{40}Ar/^{39}Ar$ data now strongly suggest this transition is not the Matuyama/Brunhes reversal per se, but rather a precursor event some 14 to 16 kyr prior to the complete reversal. It remains then to investigate the exact nature of this precursor, which previously has only been seen as paleointensity lows in deep sea sediments [*Hartl and Tauxe*, 1996]. Both sections in Quebrada Turbia are bounded by erosional surfaces or ash flows, signifying the presence of hiatuses, born out by the $^{40}Ar/^{39}Ar$ dating. In section QTW-10 one reverse polarity flow appears above the ash flow and below the transitional flows. Section QTW-11 contains several normal polarity flows above the transitional ones, prior to the appearance of an ash unit and subsequent younger flows above. Although field observations and geochemical data indicate some of the flows in the upper part of QTW-10 may be the same as flows in the middle part of QTW-11, it is difficult to produce a flow to flow correlation. The minimum number of transition flows, using the chemical correlations shown in Figure 11 is 21, assuming that all of the upper part of QTW 10 is also represented in QTW 11.

[37] One possible scenario for the precursor is motion of the transitional field to the subequatorial Australasia position, lingering there for a short but undetermined time, and then direct movement to the normal position. This necessitates a return to reverse polarity in short order to allow for the actual reversal to commence. It may just be fortuitous that no lavas were erupted during the time when the field was moving from reversed to the Australian region and then north to the normal position, and other transitional directions were not recorded. The three normal sites above the transition have similar chemistry to those in the transition, and the lowermost of these flows has an age similar to the transitional flows, but that also overlaps the age of the M-B reversal. Thus it is possible that the normal directions recorded in the top of QTW 11 are not related to the precursor, but instead are three normal directions after the full reversal.

[38] The duration of volcanic activity of the Quebrada Turbia lavas is difficult to ascertain. *Singer et al.* [1997] estimate that Qqt lavas represent some 1.8 km^3 of material. Using minimum and maximum bounds on eruption rates estimated by *Singer et al.* [1997] for the Tatara-San Pedro Complex, the Qqt lavas could represent between 6 and 30 kyr of volcanic activity. Moreover, a survey of other well-dated arc volcanoes [e.g., *Hildreth and Lanphere*, 1994; *Hildreth et al.*, 2002] suggests that it would be unusual if the entire volume of Qqt basaltic andesitic lava flows erupted over a period of less than 2 to 3 kyr. Although extraordinarily rapid magnetic field variations are suggested to occur during some reversals [*Coe and Prévot*, 1989], the opposite situation of the field concentrated within a single region during a reversal for perhaps a few kyr has not been substantiated.

[39] Records of reversals have long been sought by paleomagnetists, but due to the extremely short duration of transitions, the likelihood of finding detailed reversal sections in lavas is rare [*Coe and Glen*, 2004]. Thus it is interesting to compare the Chile data to the few records of the Matuyama/Brunhes reversal from other parts of the world. When *Clement* [1991] made his comparison of M/B records he found 21 salient studies in the literature. *Love and Mazaud* [1997] started with a database of 62 distinct records, but after applying stringent but necessary criteria, were left with only 11 individual data sets. This compilation, MBD97, has poles from four lava sites, one loess site, three shallow marine sites, and three deep-sea sites; preliminary data from QTW-10 [*Brown et al.*, 1994] is included in this compilation as one of the lava sites. From analysis of the 11 studies, *Love and Mazaud* [1997] conclude that there is support for the confinement of transitional poles to two longitudinal bands, one through the Americas, the other through Australia and East Asia, as has been suggested by earlier studies [*Clement*, 1991; *Laj et al.*, 1991]. *Hoffman* [2000] uses the MBD97 data to investigate temporal aspects of this reversal, reiterating the presence of clusters of transitional poles representing quasi-stationary positions of the field, and noting the absence of poles in the equatorial region. More recently, *Hoffman and Singer* [2004] analyzed recordings of field reversals or excursions over the last several million years, including the Chile data of *Brown et al.* [1994], and argue that whenever the axial dipole becomes weakened, a large region of the earth's surface centered about Australasia becomes dominated by a net concentration of magnetic flux beneath Australia, possibly owing to a long-lived heterogeneity in the lowermost mantle in this region.

[40] Since the late 1990s only a few studies have been published that adhere to the strict criteria of *Love and Mazaud* [1997]. These include deep-sea sedimentary results from ODP sites south of Iceland [*Channell and Lehman*, 1997; *Channell and Kleiven*, 2000] which produced detailed records from three parallel cores showing five equatorial crossings during the transition, and lava results from La Palma, Canary Islands [*Singer et al.*, 2002], with five transitional directions from one continuous section. Additional data has been provided from Guadeloupe Island in the French West Indies [*Carlut et al.*, 2000] but these three superimposed lavas with T-R-N directions do not pass the criteria outlined by *Love and Mazaud* [1997]. Results from Maui reveal a R-N-T-N pattern with three equatorial crossings, one over the Americas and two in the Western Pacific [*Coe et al.*, 2004].

[41] From the above discussion of $^{40}Ar/^{39}Ar$ geochronology it appears that of the igneous records only the Hawaiian record truly represents the Matuyama-Brunhes reversal, whereas the other studies, Tahiti, Chile, and La Palma, represent at least in part the precursor event. The paleomagnetic poles from Tahiti [*Chauvin et al.*, 1990] also lie in the Australasia region, with only positions south of the equator represented. At face value, the Tahiti and Chile recordings of mono-directional transition fields near Australia near the time of the M-B reversal support the hypothesis of *Hoffman and Singer* [2004] that a mantle

heterogeneity below Australia—a region of fast seismic velocities and a thickened D″ layer—has had a profound filtering influence over the observed field at the surface for at least the last several million years. The La Palma section [*Singer et al.*, 2002] is more complicated and appears to record transitional directions from both the precursor and the M-B reversal; precursor poles fall in the southern hemisphere but there is no preference for Australasia seen until the reversal itself. These observations are also consistent with the *Hoffman and Singer* [2004] hypothesis in which the distance of a site away from the Australasia flux concentration, and the magnitude of changes in field intensity, will determine whether transitional VGPs concentrate near Australia, or the South America-South Atlantic region.

[42] Notably, only the detailed study of the Haleakala caldera section on Maui [*Coe et al.*, 2004] yields 24 transitional flows of bona fide Matuyama-Brunhes age and a complex pattern of poles located first over the Americas and later dipping southward to New Zealand before returning to the normal position. Although quite surprising, three of the four a lava records that have been thought for the past decade to record the Matuyama-Brunhes reversal, seem now to be more consistent with their recording a precursor event and not the actual polarity switch.

7. Conclusions

[43] Our investigation of the paleomagnetism and $^{40}Ar/^{39}Ar$ geochronology of the unusual lava sequence at the Tatara San Pedro volcanic complex leads to the following conclusions:

[44] 1. Paleomagnetic directions from two sections in Quebrada Turbia on the north side of the complex yield a record of reversed, transitional and normal directions from flows of the Quebrada Turbia unit. The southern section, QTW-10, consists of 11 flows with a lowermost flow of the older Munoz sequence overlain by an ash layer and then one reversed flow followed by nine transitional flows. The sequence is topped by a thick ash layer above which are much younger overlying flows. The northern section, QTW-11 comprises 20 flows lying directly on a rhyolitic block and ash layer that rests on basement rocks. The first 17 flows are transitionally magnetized with the top three flows being normal, separated from younger overlying flows by an ash layer. Characteristic directions of the transitional flows, determined via detailed alternating field demagnetization, are all very similar. The VGPs cluster over Australia with a mean pole for the transitional flows of 22.7°S and 135.7°E with a circle of confidence of 4.2°.

[45] 2. Twenty-one new $^{40}Ar/^{39}Ar$ incremental heating experiments, combined with those from the earlier study of *Singer and Pringle* [1996], yield well-defined and overlapping isochron ages from nine of the transitionally magnetized lavas. The weighted mean of these nine isochron ages yield an age for the period of transitional magnetization recorded in the flow sequence in Quebrada Turbia of 791.7 ± 3.0 ka where the 2 sigma uncertainty reflects analytical contributions only. This age is significantly older than both the best radioisotopic and astrochronologic ages of 776 ± 2 and 778 ± 4 ka, respectively, for the M-B reversal. It is, however, indistinguishable from a 793 ka event known previously only from low paleointensities recorded in deep marine sediments, which, on the basis of astrochronologic dating, preceded the M-B reversal by about 15 kyr. Thus, rather than recording the M-B reversal as has been inferred by us in the past [*Brown et al.*, 1994; *Singer and Pringle*, 1996], the Quebrada Turbia lavas most likely record a part of the same precursor evinced globally by the marine paleointensity records.

[46] 3. Radioisotopic dating using the $^{40}Ar/^{39}Ar$ incremental heating method on multiple subsamples from many transitionally magnetized lavas comprising flow sequences is critical to delineating the volcanic record of past magnetic field behavior [e.g., *Coe et al.*, 2004]. More specifically, a precision level of better than 1.0% at the 95% confidence level was essential to recognizing for the first time the possibility that the Quebrada Turbia lavas may record an excursion at 792 ka that preceded the M-B reversal by about 14-6 kyr.

[47] 4. The observation that transitional VGPs potentially associated with the precursor event at volcanic sites in Tahiti and Chile cluster near Australasia, whereas those from La Palma, a site much farther from Australia, lie near South America, is consistent with the hypothesis of *Hoffman and Singer* [2004] whereby lower mantle heterogeneity beneath Australia dominates the weakened field during reversals or excursions at sites proximal to Australia, but the ability of this unusual mantle domain to concentrate and retain magnetic flux diminishes with distance from Australia. Further analysis of these and other records will be necessary to characterize more thoroughly the paleomagnetic changes that transpired during and after the precursor event and to determine how these are related to the final directional change associated with the M-B reversal.

[48] **Acknowledgments.** This study, including the writing, was funded by the National Science Foundation (grants EAR-9017690 and EAR-9316544 to L. B. and EAR-9909309, EAR-0114055, and EAR-033768403 to B. S.), a Geological Society of America Student Research award to J. P., and an Institute for Rock Magnetism research award. Geochemical data supplied by Andrew Wulff. Special recognition is deserved by all our colleagues in the Tatara-San Pedro project, Michael Dungan, Fred Frey, Mike Rhodes, Wes Hildreth, Bob Drake, Lyn Gualtieri, Kathy Ervin, Steve Caunt, Leo Lopez-Escobar, Jorge Lobato, Ren Thompson, Todd Feeley, Steve Nelson, John Davidson, and Teresa Boundy, who contributed to this effort. An earlier version of this manuscript benefited from comments by Ron Merrill, Ed Mankinen, and Emilio Herrero-Bervera. B. Singer also thanks Ken Hoffman for sharing ideas and discussing this work over many years. Comments from Rob Coe, an anonymous reviewer and an anonymous associate editor did much to improve this manuscript, including convincing us to seriously consider the M-B precursor.

References

Baksi, A. K., V. Hsu, M. O. McWilliams, and E. Farrar (1992), $^{40}Ar/^{39}Ar$ dating of the Brunhes-Matuyama geomagnetic field reversal, *Science*, *256*, 356–357.

Brown, L., J. Pickens, and B. Singer (1994), Matuyama-Brunhes transition recorded in lava flows of the Chilean Andes: Evidence for dipolar fields during reversals, *Geology*, *22*, 299–302.

Carlut, J., X. Quiduelleur, V. Courtillot, and G. Boudon (2000), Paleomagnetic directions and K/Ar dating of 0 to 1 Ma lava flows from La Guadeloupe Island (French West Indies): Implications for time-averaged field models, *J. Geophys. Res.*, *105*, 835–849.

Channell, J. E. T., and H. F. Kleiven (2000), Geomagnetic paleointensities and astrochronological ages for the Matuyama-Brunhes boundary and the boundaries of the Jaramillo Subchron: Paleomagnetic and oxygen isotope records from ODP Site 983, *Philos. Trans. R. Soc. London, Ser. A*, *358*, 1027–1047.

Channell, J. E. T., and B. Lehman (1997), The last two geomagnetic polarity reversals recorded in high-deposition-rate sedimentary drifts, *Nature*, *389*, 712–715.

Chauvin, A., P. Roperch, and R. A. Duncan (1990), Records of geomagnetic reversals from volcanic islands of French Polynesia: 2. Paleomagnetic study of a flow sequence (1.2–0.6 Ma) from the island of Tahiti and discussion of reversal models, *J. Geophys. Res.*, *95*, 2727–2752.

Clement, B. M. (1991), Geographical distribution of transitional VGPs: Evidence for non-zonal equatorial symmetry during the Matuyama-Brunhes geomagnetic reversal, *Earth Planet. Sci. Lett.*, *104*, 48–58.

Clement, B. M. (2004), Dependence of the duration of geomagnetic polarity reversals on site latitude, *Nature*, *428*, 637–640.

Coe, R. S., and J. M. G. Glen (2004), The complexity of reversals, in *Timescales of the Paleomagnetic Field*, *Geophysical Monograph Series*, edited by J. E. T. Channell et al., AGU, Washington, D. C., in press.

Coe, R. S., and M. Prévot (1989), Evidence suggesting extremely rapid field variation during a geomagnetic reversal, *Earth Planet. Sci. Lett.*, *92*, 292–298.

Coe, R. S., L. Hongre, and G. A. Glatzmaier (2000), An examination of simulated geomagnetic reversals from a paleomagnetic perspective, *Philos. Trans. R. Soc. London, Ser. A*, *358*, 1141–1170.

Coe, R. S., B. S. Singer, M. S. Pringle, and X. Zhao (2004), Matuyama-Brunhes reversal and Kamikatsura event on Maui: Paleomagnetic directions and $^{40}Ar/^{39}Ar$ ages, *Earth Planet. Sci. Lett.*, *222*, 667–684.

Day, R., M. Fuller, and V. A. Schmidt (1977), Hysteresis properties of titanomagnetites: Grain size and composition dependence, *Phys. Earth Planet. Inter.*, *13*, 260–267.

Duffield, W. A., and G. B. Dalrymple (1990), Taylor Creek rhyolite of New Mexico, a rapidly emplaced field of domes and flows, *Bull. Volcanol.*, *52*, 475–487.

Dungan, M., et al. (1992), The life history of an Andean volcano, *Eos Trans. AGU*, *73*, 642–643.

Dungan, M. A., A. Wulff, and R. Thompson (2001), Eruptive stratigraphy of the Tatara-San Pedro Complex, 36°S, Southern Volcanic Zone, Chilean Andes: Reconstruction method and implications for magma evolution at long-lived arc volcanic centers, *J. Petrol.*, *42*, 555–626.

Ferguson, K. M., M. A. Dungan, J. P. Davidson, and M. T. Colucci (1992), The Tatara-San Pedro volcano, 36S, Chile: A chemically variable, dominantly mafic magmatic system, *J. Petrol.*, *33*, 1–43.

Fisher, R. A. (1953), Dispersion on a sphere, *Proc. R. Soc. London, Ser. A*, *217*, 295–305.

Glatzmaier, G. A., and P. H. Roberts (1995), A three-dimensional self-consistent computer simulation of a geomagnetic field reversal, *Nature*, *377*, 203–209.

Glatzmaier, G. A., R. S. Coe, L. Hongre, and P. H. Roberts (1999), The role of the Earth's mantle in controlling the frequency of geomagnetic reversals, *Nature*, *401*, 885–890.

Hartl, P., and L. Tauxe (1996), A precursor to the Matuyama/Brunhes transition-field instability as recorded in pelagic sediments, *Earth Planet. Sci. Lett.*, *138*, 121–135.

Hildreth, W., and M. Lanphere (1994), Potassium-argon geochronology of a basalt-andesite-dacite arc system: The Mount Adams volcanic field, Cascade Range of southern Washington, *Geol. Soc. Am. Bull.*, *106*, 1413–1429.

Hildreth, W., J. Fierstein, and M. Lanphere (2002), Eruptive history and geochronology of the Mount Baker volcanic field, Washington, *Geol. Soc. Am. Bull.*, *115*, 729–764.

Hoffman, K. A. (1992), Dipolar reversal states of the geomagnetic field and core-mantle dynamics, *Nature*, *359*, 789–794.

Hoffman, K. A. (1996), Transitional paleomagnetic field behavior: Preferred paths or patches, *Surv. Geophys.*, *17*, 207–211.

Hoffman, K. A. (2000), Temporal aspects of the last reversal of Earth's magnetic field, *Philos. Trans. R. Soc. London, Ser. A*, *358*, 1181–1190.

Hoffman, K. A., and B. Singer (2004), Regionally recurrent paleomagnetic transitional fields and mantle processes, in *Timescales of the Paleomagnetic Field*, *Geophysical Monograph Series*, edited by J. E. T. Channell et al., AGU, Washington, D. C., in press.

Izett, G. A., and J. D. Obradovich (1994), $^{40}Ar/^{39}Ar$ age constraints for the Jaramillo normal subchron and the Matuyama-Brunhes geomagnetic boundary, *J. Geophys. Res.*, *99*, 2925–2934.

Kent, D. V., and D. A. Schneider (1995), Correlation of paleointensity variation records in the Brunhes/Matuyama polarity transition interval, *Earth Planet. Sci. Lett.*, *129*, 135–6144.

Kuang, W., and J. Bloxham (1997), An Earth-like numerical dynamo model, *Nature*, *389*, 371–374.

Laj, C., A. Mazaud, R. Weeks, M. Fuller, and E. Herrero-Bervera (1991), Geomagnetic reversal paths, *Nature*, *351*, 447.

Love, J. J., and A Mazaud (1997), A database for the Matuyama-Brunhes magnetic reversal, *Phys. Earth Planet. Inter.*, *103*, 207–245.

Merrill, R. T., and P. L. McFadden (1999), Geomagnetic polarity transitions, *Rev. Geophys.*, *37*, 201–226.

Prevot, M., and P. Camps (1993), Absence of preferred longitude sectors for poles from volcanic records of geomagnetic reversals, *Nature*, *366*, 53–57.

Renne, P. R., C. C. Swisher, A. L. Deino, D. B. Karner, T. L. Owens, and D. J. DePaolo (1998), Intercalibration of standards, absolute ages and uncertainties in $^{40}Ar/^{39}Ar$ dating, *Chem. Geol.*, *145*, 117–152.

Rhodes, J. M. (1988), Geochemistry of the 1984 Mauna Loa eruption: Implications for magma storage and supply, *J. Geophys. Res.*, *93*, 4453–4460.

Schneider, D. A., D. V. Kent, and G. A. Mello (1992), A detailed chronology of the Australasian impact event, the Brunhes-Matuyama geomagnetic polarity reversal, and global climate change, *Earth Planet. Sci. Lett.*, *111*, 395–405.

Shackleton, N. J., A. Berger, and W. R. Peltier (1990), An alternative astronomical calibration of the lower Pleistocene timescale based on OPD site 677, *Trans. R. Soc. Edinburgh Earth Sci.*, *81*, 251–261.

Singer, B., and M. Pringle (1996), Age and duration of the Matuyama-Brunhes geomagnetic polarity reversal from $^{40}Ar/^{39}Ar$ incremental heating analyses of lavas, *Earth Planet. Sci. Lett.*, *139*, 47–61.

Singer, B. S., R. A. Thompson, M. A. Dungan, T. C. Feeley, S. T. Nelson, J. C. Pickens, L. L. Brown, A. W. Wulff, J. P. Davidson, and J. Metzger (1997), Volcanism and erosion during the past 930 k. y. at the Tatara-San Pedro Complex, Chilean Andes, *Geol. Soc. Am. Bull.*, *109*, 127–142.

Singer, B. S., M. K. Relle, K. A. Hoffman, A. Battle, C. Laj, H. Guillou, and J. C. Carracedo (2002), Ar/Ar ages of transitionally magnetized lavas on La Palma, Canary Islands, and the geomagnetic instability timescale, *J. Geophys. Res.*, *107*(B11), 2307, doi:10.1029/2001JB001613.

Spell, T. L., and I. McDougall (1992), Revisions to the age of the Matuyama-Brunhes boundary and the Pleistocene polarity timescale, *Geophys. Res. Lett.*, *19*, 1181–1184.

Steiger, R. H., and E. Jäger (1977), Subcommission on geochronology: Convention on the use of decay constants in geo- and cosmochronology, *Earth Planet. Sci. Lett.*, *36*, 359–362.

Tauxe, L., T. Herbert, N. J. Shackleton, and Y. S. Kok (1996), Astronomical calibration of the Matuyama-Brunhes boundary: Consequences for magnetic remanence acquisition in marine carbonates and the Asian loess sequences, *Earth Planet. Sci. Lett.*, *140*, 133–146.

Taylor, J. R. (1982), *An Introduction to Error Analysis: The Study of Uncertainties in Physical Measurements*, 270 pp., Univ. Sci. Books, Mill Valley, Calif.

Tric, E., C. Laj, C. Jehanno, J.-P. Valet, C. Kissel, A. Mazaud, and S. Iaccarino (1991), High resolution record of the Upper Olduvai transition from the Po valley (Italy) sediments: Support for a dipolar transition geometry?, *Phys. Earth Planet. Inter.*, *65*, 319–336.

Valet, J.-P., P. Tucholka, V. Courtillot, and L. Meynadier (1992), Paleomagnetic constraints on the geometry of the geomagnetic field during reversals, *Nature*, *356*, 400–407.

Wijbrans, J. R., M. S. Pringle, A. A. P. Koppers, and R. Scheveers (1995), Argon geochronology of small samples using the Vulkaan argon laserprobe, *Proc. Dutch Acad. Sci.*, *98*, 185–218.

Wulff, A. H. (1998), The chemical evolution of Volcan Tatara-san Pedro, 36°S, Southern Volcanic Zone, Chile, Ph.D. dissertation, 435 pp., Univ. of Mass., Amherst.

York, D. (1969), Least squares fitting of a straight line with correlated errors, *Earth Planet. Sci. Lett.*, *5*, 320–324.

L. L. Brown, Department of Geosciences, University of Massachusetts, Amherst, MA 01003, USA. (lbrown@geo.umass.edu)

J. C. Pickens, Structure Seal Gravity Mechanics Core Group, ExxonMobile Exploration, 233 Benmar (GP3-706), Houston, TX 77060, USA. (jim.c.pickens@exxonmobile.com)

B. R. Jicha and B. S. Singer, Department of Geology and Geophysics, University of Wisconsin, Madison, WI 53706, USA. (bjicha@geology.wisc.edu; bsinger@geology.wisc.edu)

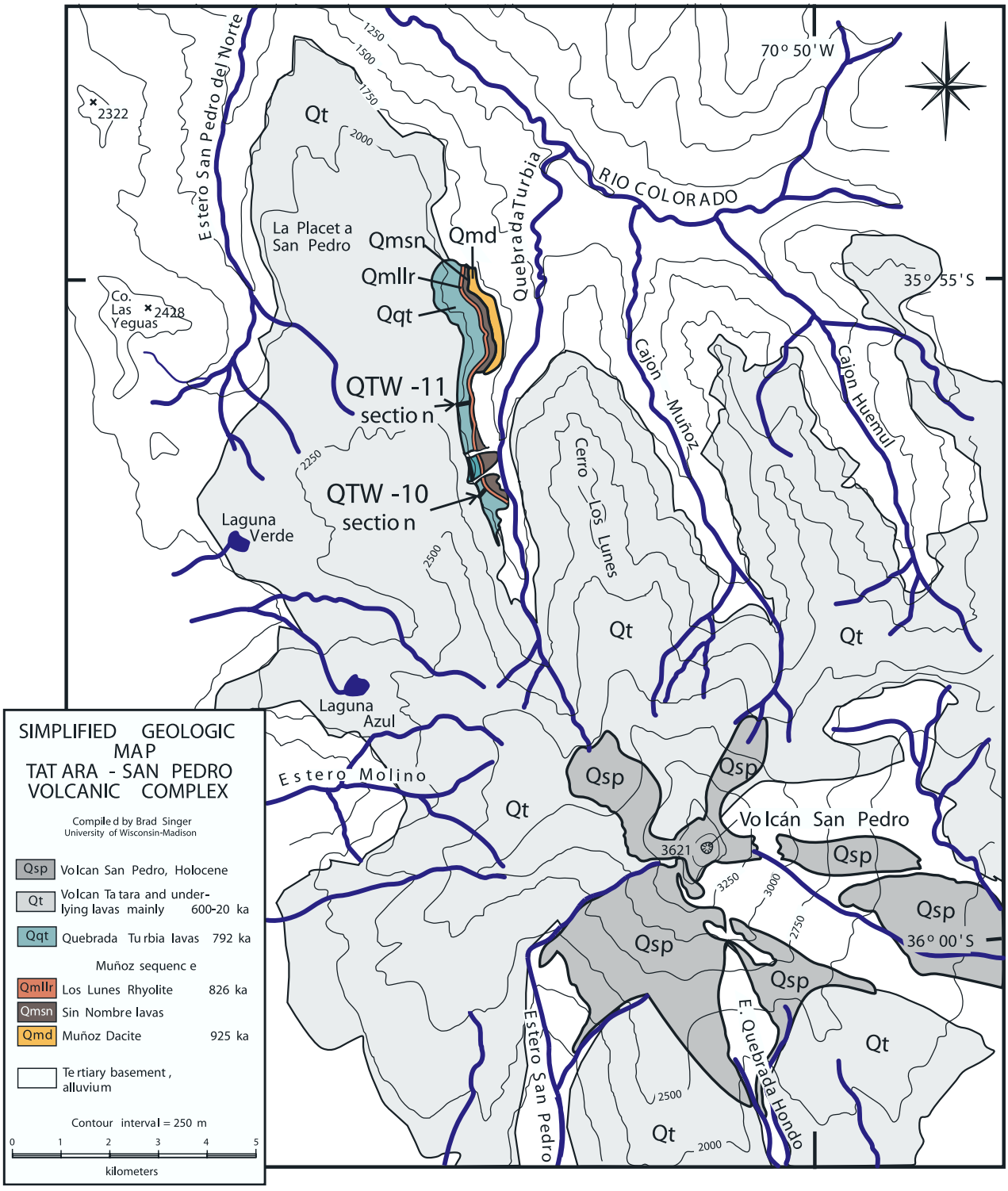

Figure 2. Simplified geologic map of the Tatara-San Pedro volcanic complex, Chile. Locations of sections QTW-10 and QTW-11, discussed in the text, are indicated by arrows. Map is modified from *Singer et al.* [1997].

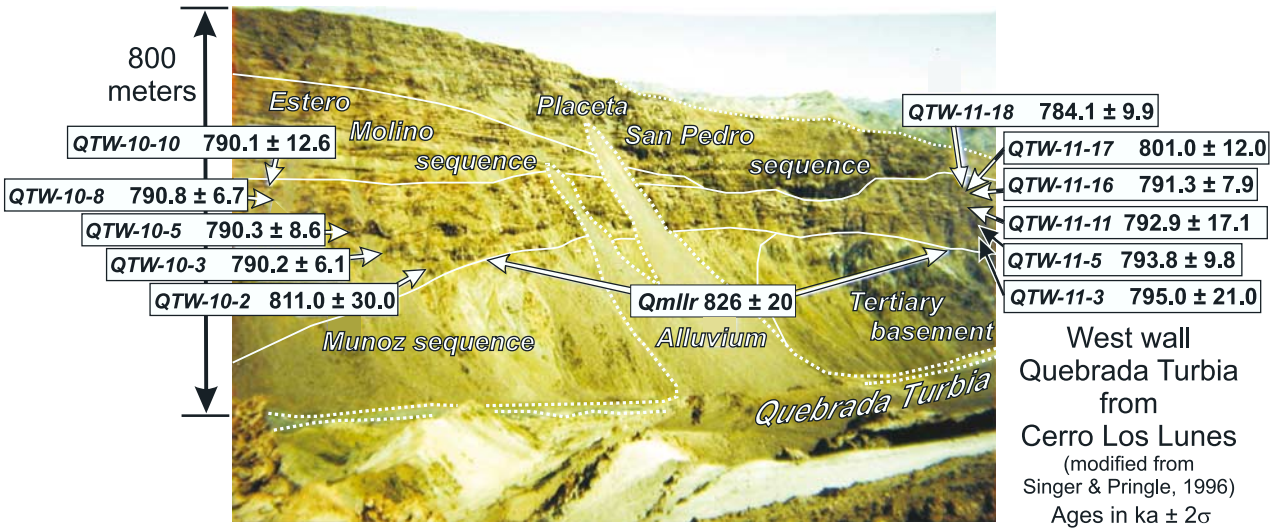

Figure 3. Photograph of the west wall of Quebrada Turbia. Vertical relief from the valley floor to ridge is ~800 m. Sequences above and below the Quebrada Turbia sequence are labeled. Location of 12 radioisotopic age determinations and associated paleomagnetic sites are indicated. Paleomagnetic sites are numbered from the bottom up; section QTW-10, sites 10-1 to 10-11 are on the left, and section QTW-11, sites 11-1 to 11-20 are on the right and were collected in traverses joining and coincident with the radioisotopic locations. See Table 2 for additional information on the age determinations.